NASA
Contractor Report 4757

Army Research Laboratory
Technical Report ARL–CR–312

Local Synthesis and Tooth Contact Analysis of Face-Milled, Uniform Tooth Height Spiral Bevel Gears

F.L. Litvin and A.G. Wang

GRANT NAG3–1607
OCTOBER 1996

National Aeronautics and
Space Administration

NASA
Contractor Report 4757

Army Research Laboratory
Technical Report ARL–CR–312

Local Synthesis and Tooth Contact Analysis of Face-Milled, Uniform Tooth Height Spiral Bevel Gears

F.L. Litvin and A.G. Wang
University of Illinois at Chicago
Chicago, Illinois

Prepared for
Vehicle Propulsion Directorate
U.S. Army Research Laboratory
and
Lewis Research Center
under Grant NAG3–1607

National Aeronautics and
Space Administration
Office of Management
Scientific and Technical
Information Program
1996

LOCAL SYNTHESIS AND TOOTH CONTACT ANALYSIS OF FACE-MILLED, UNIFORM TOOTH HEIGHT SPIRAL BEVEL GEARS

by

F. L. Litvin[1] and A. G. Wang[2]
Department of Mechanical Engineering
University of Illinois at Chicago
Chicago, IL

ABSTRACT

Face-milled spiral bevel gears with uniform tooth height are considered. An approach is proposed for the design of low-noise and localized bearing contact of such gears. The approach is based on the mismatch of contacting surfaces and permits two types of bearing contact either directed longitudinally or across the surface to be obtained. Conditions to avoid undercutting were determined. A Tooth Contact Analysis (TCA) was developed. This analysis was used to determine the influence of misalignment on meshing and contact of the spiral bevel gears. A numerical example that illustrates the theory developed is provided.

[1]Dr. Professor, Principal Investigator
[2]Research Assistant

TABLE OF CONTENTS

NOMENCLATURE

α_g	Blade angle of gear head cutter (fig. 4)(Table 2)
α_p	Profile angle of pinion head cutter (figs. 7, 18)(Table 3)
γ_1, γ_2	Angles of pinion and gear pitch cone, respectively (figs. 6, 11, 12)(Table 1)
γ	Shaft angle (Table 1)
η_1	Tangent to the path of contact on the pinion surface (Table 3)
θ_p	Surface parameter of the pinion head cutter
θ_g	Surface parameter of the gear head cutter
λ_p	Surface parameter of the pinion head cutter (figs. 7, 18)
σ_{12}	Angle formed between principal direction $\mathbf{e}_f$ and $\mathbf{e}_s$ (fig. 10)
ϕ_i $(i = 1, 2)$	Angle of rotation of the pinion $(i = 1)$ or gear $(i = 2)$ in the process of meshing (figs. 11, 13, 14, 15)
ψ_{c_i} $(i = 1, 2)$	Angle of rotation of the cradle in the process for generation of the pinion $(i = 1)$ or gear $(i = 2)$ (fig. 5)
ψ_i $(i = 1, 2)$	Angle of rotation of the pinion $(i = 1)$ or gear $(i = 2)$ in the process for generation (figs. 6, 8)
ω_i $(i = 1, 2)$	Angular velocity of the pinion $(i = 1)$ or gear $(i = 2)$ (in meshing and generation)
ω_{c_i} $(i = 1, 2)$	Angular velocity of the cradle for the generation of the pinion $(i = 1)$ or gear $(i = 2)$
Σ_i $(i = 1, 2)$	Pinion $(i = 1)$ or gear $(i = 2)$ tooth surface (fig. 17)
Σ_{t_i} $(i = 1, 2)$	Pinion $(i = 1)$ or gear $(i = 2)$ generating surface (figs. 1, 2, 3, 16)
ΔA_p, ΔA_g	Pinion and gear axial displacements, respectively (figs. 11, 13)(Table 4)
ΔE, $\Delta\gamma$	Errors the offset and shaft angle, respectively (figs. 12, 13)(Table 4)

$\Delta\phi_2(\phi_1)$	Function of transmission errors (figs. 14, 15)
$\mathbf{e}_f, \mathbf{e}_h, \mathbf{e}_s, \mathbf{e}_q$	Unit vectors of principal directions of pinion and gear tooth surface, respectively (fig. 10)
h_d	Dedendum height of the pinion
k_f, k_h, k_s, k_q	Principal curvatures of the pinion and gear tooth surfaces, respectively
$\mathbf{L}_{ji}$	Matrix of orientation transformation from system S_i to system S_j (3X3)
m'_{21}	Derivative of $\phi_2(\phi_1)$ (Table 3)
M	Mean contact point (figs. 1, 2, 3, 7, 9)(Table 3)
$\mathbf{M}_{ji}$	Matrix of coordinate transformation from system S_i to system S_j (4X4)
$\mathbf{n}_{k_i}$, $\mathbf{N}_{k_i}$	Unit normal and normal to the generating surface Σ_i represented in coordinate system S_k
N_i $(i = 1, 2)$	Number of teeth of pinion $(i = 1)$ and gear $(i = 2)$ (Table 1)
q_i $(i = 1, 2)$	Installment angle for the head cutter of the pinion $(i = 1)$ and gear $(i = 2)$ (fig. 5)(Tables 2, 3)
R_1	Radius of the generating surface of revolution for the pinion (figs. 3, 7, 16, 18)(Table 3)
R_p, R_g	Radius of the head-cutter at mean point for the pinion and gear (figs. 1, 2, 3, 4, 7, 16, 18)(Tables 2, 3)
$\mathbf{r}_i$	Position vector in system S_i $(i = 1, 2, h, t_1, t_2)$
S_{r_i} $(i = 1, 2)$	Radial setting of the head cutter of the pinion $(i = 1)$ and gear $(i = 2)$ (fig. 5)(Tables 2, 3)
S_i	Coordinate system
$\mathbf{v}_r^{(t_i)}$ $(i = 1, 2)$	Velocity of contact point in its motion over surface Σ_{t_i}
$\mathbf{v}^{(ij)}$	Relative velocity at contact point $(i, j = 1, 2, c_1, c_2, t_1, t_2)$
$v_s^{(1)}$, $v_q^{(1)}$	Components of the velocity of the contact point in its motion over Σ_1

1 Introduction

Two models for spiral bevel gears with uniform tooth height were proposed by Litvin et al. [1]. The generation of tooth surfaces of such gears is based on application: (i) of two cones that are in tangency along their common generatrix (model 1), and (ii) a cone and a surface of revolution that are in tangency along a common circle (model 2). The pinion and the gear are face-milled by head-cutters whose blades by rotation form the generating surfaces.

The generating surfaces provide conjugate pinion-gear tooth surfaces with a localized bearing contact that is formed by a set of instantaneous contact ellipses. The path of contact is directed across the surfaces in model 1 (fig. 1), and in the longitudinal direction in model 2 (fig. 2). The transmission errors are zero but only for aligned gear drives.

It is well known that misalignment of a gear drive causes a shift of the bearing contact and transmission errors. The transmission errors are one of the main sources of vibration. Therefore, the direct application of the models discussed above for generating surfaces is undesirable.

It was discovered that misalignment of a gear drive causes an almost linear but discontinuous transmission function. However, such functions can be absorbed by a predesigned parabolic function of transmission errors. The interaction of the parabolic function and a linear function results a parabolic function with the same parabola coefficient [2]. Based on this consideration, it becomes necessary to modify the process discussed above for generation to obtain a predesigned parabolic function of transmission errors. It was proposed in the work [3] to obtain the desired parabolic function of transmission errors by executing proper nonlinear relations between the motions of the cradle and the gear (or the pinion) being generated. This approach requires the application of the CNC machines.

The purpose of this report is to propose modifications of generating surfaces that will obtain: (i) a localized bearing contact that may be directed in the longitudinal direction or across the surface, and (ii) a predesigned parabolic function. These goals, that will be

proven later, are obtained by the proper mismatch of the ideal generating surfaces shown in figs. 1 and 2. The mismatch of surfaces is achieved by application of modified generating surfaces shown in fig. 3. The modified generating surfaces are in point contact instead of tangency along a line that the ideal generating surfaces have. The desired parabolic function of transmission errors, the orientation of the path of contact, and the magnitude of the major axis of the contact ellipses are obtained by the proper determination of the curvature and the mean radius of the surface of revolution of the generating tool.

Design of drives with a small number of pinion teeth may be accompanied with pinion undercutting. Using the approach proposed in [7, 8, 9], it becomes possible to avoid undercutting of spiral bevel pinions. The meshing and contact of the tooth surfaces was simulated by the TCA (Tooth Contact Analysis) computer program developed by the authors.

The contents of the report cover the following topics:

(1) Method for generation of conjugate pinion-gear tooth surfaces.

(2) Derivation of gear and pinion tooth surfaces.

(3) Local synthesis as the tool for the directed mismatch of contacting surfaces.

(4) Simulation of meshing and contact of misaligned drives.

(5) Avoidance of pinion undercutting.

Numerical examples for the illustration of the proposed approach are considered.

2 Method for Generation of Conjugated Pinion-Gear Tooth Surfaces

Gear Generation:

The head-cutter for gear generation is provided with inner and outer straight-line blades (fig. 4), that form two cones while the blades are rotated about the Z_{t_2}-axis of the head cutter. These cones will generate the convex and concave sides of the gear profile, respectively [12].

We apply coordinate systems S_{c_2}, S_2, S_m that are rigidly connected to the cradle of the generating machine, the gear and the cutting machine, respectively (figs. 5 and 6). The cradle with coordinate system S_{c_2} performs rotation about the Z_m-axis, and ψ_{c_2} is the current angle of rotation of the cradle (We take $i = 2$ in the designations of fig. 5). Coordinate system S_{t_2} is rigidly connected to the gear head-cutter that is mounted on the cradle. The installment of the head-cutter is determined with angle q_2 and $S_{r_2} = \left|\overline{O_{c_2}O_{t_2}}\right|$ (fig. 5(b)). The gear in the process for generation performs rotation about the Z_b-axis of the auxiliary fixed coordinate system S_b that is rigidly connected to the S_m coordinate system (fig. 6). The installment of S_b with respect to S_m is determined with angle γ_2, where γ_2 is the angle of the gear pitch cone. The current angle of gear rotation is ψ_2 (fig. 6). Angles ψ_{c_2} and ψ_2 are related as

$$\frac{\psi_{c_2}}{\psi_2} = \frac{\omega_{c_2}}{\omega_2} = \sin\gamma_2 \tag{1}$$

The observation of this equation guaranties that the X_m-axis is the instantaneous axis of rotation of the gear in its relative motion with respect to the cradle.

Pinion Generation:

The head-cutters for pinion generation are provided with separate blades that will generate the convex and concave sides of the pinion profile, respectively (fig. 7). The pinion generating tool is installed on the cradle similarly to the installment of the gear generating cone (We take $i = 1$ in the designations of fig. 5). An auxiliary fixed coordinate system

S_a is rigidly connected to the S_m coordinate system (fig. 8). An imaginary process for the pinion generation for the purpose of simplification of the TCA program is considered. The installment of coordinate system S_a with respect to S_m is determined in the real process of cutting by the angle γ_1 that is measured clockwise, opposite to the direction shown in fig. 8. The pinion performs rotation about the Z_a-axis and ψ_1 is the current angle of rotation. The angles of rotation of the pinion and the cradle are related as

$$\frac{\psi_{c_1}}{\psi_1} = \frac{\omega_{c_1}}{\omega_1} = \sin\gamma_1 \tag{2}$$

Axis X_m in accordance to equation (2) is the instantaneous axis of rotation of the pinion in its relative motion with respect to the cradle.

3 Derivation of Gear Tooth Surface

Equations of Gear Generating Surface

We consider that the gear head-cutter surface is represented in S_{t_2} (fig. 4) by vector function $\mathbf{r}_{t_2}(s_g, \theta_g)$

$$\mathbf{r}_{t_2}(s_g, \theta_g) = \begin{bmatrix} (R_g - s_g \sin\alpha_g)\cos\theta_g \\ (R_g - s_g \sin\alpha_g)\sin\theta_g \\ s_g \cos\alpha_g \end{bmatrix} \tag{3}$$

where s_g and θ_g are the surface coordinates; α_g is the blade angle; R_g is the radius of the head-cutter at the mean point. Equations (3) may also represent the convex side of the generating cone considering that α_g is negative.

Coordinate system S_{t_2} is rigidly connected to coordinate system S_{c_2}, and the unit normal to the gear generating surface is represented by the equations

$$\mathbf{n}_{c_2}(\theta_g) = \frac{\mathbf{N}_{c_2}}{|\mathbf{N}_{c_2}|}, \quad \mathbf{N}_{c_2} = \frac{\partial \mathbf{r}_{t_2}}{\partial \theta_g} \times \frac{\partial \mathbf{r}_{t_2}}{\partial s_g} \tag{4}$$

Equations (3) and (4) yield

$$\mathbf{n}_{c_2}(\theta_g) = \begin{bmatrix} \cos\alpha_g \cos\theta_g \\ \cos\alpha_g \sin\theta_g \\ \sin\alpha_g \end{bmatrix} \tag{5}$$

Equations of the Family of Generating Surfaces in S_2

A family of tool surfaces is generated in gear coordinate system S_2 while the cradle and the mounted tool and the gear perform the rotational motions that are shown in figs. 5 and 6. The family of surfaces is represented in S_2 by the matrix equation

$$\begin{aligned} \mathbf{r}_2(s_g, \theta_g, \psi_2) &= \mathbf{M}_{2b}(\psi_2)\mathbf{M}_{bm}\mathbf{M}_{mc_2}(\psi_{c_2})\mathbf{M}_{c_2t_2}\mathbf{r}_{t_2}(s_g, \theta_g) \\ &= \mathbf{M}_{2t_2}(\psi_2)\mathbf{r}_{t_2}(s_g, \theta_g) \end{aligned} \tag{6}$$

The product of matrices $\mathbf{M}_{2t_2}$ is based on the coordinate transformations from S_{t_2} to S_2 (figs. 5 and 6), where ψ_2 and ψ_{c_2} are related by equation (1) and

$$\mathbf{M}_{2b} = \begin{bmatrix} \cos\psi_2 & \sin\psi_2 & 0 & 0 \\ -\sin\psi_2 & \cos\psi_2 & 0 & 0 \\ 0 & 0 & 1 & 0 \\ 0 & 0 & 0 & 1 \end{bmatrix} \tag{7}$$

$$\mathbf{M}_{bm} = \begin{bmatrix} \sin\gamma_2 & 0 & -\cos\gamma_2 & 0 \\ 0 & 1 & 0 & 0 \\ \cos\gamma_2 & 0 & \sin\gamma_2 & 0 \\ 0 & 0 & 0 & 1 \end{bmatrix} \tag{8}$$

$$\mathbf{M}_{mc_2} = \begin{bmatrix} \cos\psi_{c_2} & -\sin\psi_{c_2} & 0 & 0 \\ \sin\psi_{c_2} & \cos\psi_{c_2} & 0 & 0 \\ 0 & 0 & 1 & 0 \\ 0 & 0 & 0 & 1 \end{bmatrix} \tag{9}$$

$$\mathbf{M}_{c_2t_2} = \begin{bmatrix} 1 & 0 & 0 & S_{r2}\cos q_2 \\ 0 & 1 & 0 & S_{r2}\sin q_2 \\ 0 & 0 & 1 & 0 \\ 0 & 0 & 0 & 1 \end{bmatrix} \tag{10}$$

Equation of Meshing

We derive the equation of meshing between the generating surface and gear as

$$\mathbf{n}_{c_2} \cdot \mathbf{v}_{c_2}^{(c_2 2)} = f(s_g, \theta_g, \psi_2) = 0 \tag{11}$$

representing the vectors in S_{c_2}.

where $\mathbf{v}_{c_2}^{(c_2 2)}$ is the relative velocity that is represented in the coordinate system S_{c_2}. Here,

$$\mathbf{v}_{c_2}^{(c_2 2)} = \omega_{c_2}^{(c_2 2)} \times \mathbf{r}_{c_2} = (\omega_{c_2}^{(c_2)} - \omega_{c_2}^{(2)}) \times \mathbf{r}_{c_2} \tag{12}$$

where

$$\begin{aligned} \mathbf{r}_{c_2} &= \mathbf{M}_{c_2t_2}\mathbf{r}_{t_2} \\ &= \begin{bmatrix} -s_g\sin\alpha_g\cos\theta_g + B_1 \\ -s_g\sin\alpha_g\sin\theta_g + B_2 \\ s_g\cos\alpha_g \end{bmatrix} \end{aligned} \tag{13}$$

$$(\omega_{c_2}^{(c_2)} - \omega_{c_2}^{(2)}) = \begin{bmatrix} 0 \\ 0 \\ \omega_1\sin\gamma_1 \end{bmatrix} - \mathbf{L}_{c_2m}\mathbf{L}_{mb}\mathbf{L}_{b2}\begin{bmatrix} 0 \\ 0 \\ \omega_2 \end{bmatrix} = \begin{bmatrix} -N_1/N_2\cos\gamma_2\cos\psi_{c_2} \\ N_1/N_2\cos\gamma_2\sin\psi_{c_2} \\ 0 \end{bmatrix} \tag{14}$$

Using the designations

$$\left.\begin{aligned} B_1 &= R_g\cos\theta_g + S_{r2}\cos q_2 \\ B_2 &= R_g\sin\theta_g + S_{r2}\sin q_2 \end{aligned}\right\} \tag{15}$$

and considering that $N_1/N_2 = \sin\gamma_1/\sin\gamma_2$ and $|\omega_1| = 1$, we obtain from equation(12) that

$$\mathbf{v}_{c_2}^{(c_2 2)} = \begin{bmatrix} s_g\cos\gamma_2\sin\psi_{c_2}\cos\alpha_g N_1/N_2 \\ s_g\cos\gamma_2\cos\psi_{c_2}\cos\alpha_g N_1/N_2 \\ N_1/N_2\cos\gamma_2(s_g\sin\alpha_g\sin(\theta_g+\psi_{c_2}) - B_1\sin\psi_{c_2} - B_2\cos\psi_{c_2}) \end{bmatrix} \tag{16}$$

The equation of meshing (11) is represented as

$$s_g(\theta_g, \psi_{c_2}) = \frac{\sin\alpha_g(B_1 \sin\psi_{c_2} + B_2 \cos\psi_{c_2})}{\sin(\theta_g + \psi_{c_2})} \tag{17}$$

Equations of Gear Tooth Surface

Equations (6) and (17) represent the gear tooth surface by three related parameters. Taking into account that these equations are linear with respect to s_g, we may eliminate s_g and represent the gear tooth surface by two independent parameters, θ_g and ψ_2, as

$$\mathbf{r}_2 = \mathbf{r}_2(\theta_g, \psi_2) \tag{18}$$

4 Derivation of Pinion Tooth Surface

Equations of Pinion Generating Surface

The derivations are similar to those that have been described in section 3. The generating surface of revolution is represented in S_{t_1} (fig. 7) as

$$\mathbf{r}_{t_1}(\lambda_p, \theta_p) = \begin{bmatrix} [R_p - R_1(\cos\alpha_p - \cos(\alpha_p + \lambda_p))]\cos\theta_p \\ [R_p - R_1(\cos\alpha_p - \cos(\alpha_p + \lambda_p))]\sin\theta_p \\ -R_1(\sin\alpha_p - \sin(\alpha_p + \lambda_p)) \end{bmatrix} \tag{19}$$

where λ_p and θ_p are the generating surface coordinates; α_p is the profile angle at point M; R_p is the radius of the head-cutter at mean point; R_1 is the radius of the surface of revolution. Equations (19) can also represent the concave side of the generating surface of revolution if we substitute α_p as $180° - \alpha_p$.

Coordinate system S_{t_1} is rigidly connected to coordinate system S_{c_1}, and the unit normal to the pinion generating surface is represented by the equations

$$\mathbf{n}_{c_1}(\lambda_p, \theta_p) = \frac{\mathbf{N}_{c_1}}{|\mathbf{N}_{c_1}|}, \quad \mathbf{N}_{c_1} = \frac{\partial \mathbf{r}_{t_1}}{\partial \theta_p} \times \frac{\partial \mathbf{r}_{t_1}}{\partial \lambda_p} \tag{20}$$

Equations (19) and (20) yield

$$\mathbf{n}_{c_1}(\lambda_p, \theta_p) = \begin{bmatrix} \cos\theta_p \cos(\alpha_p + \lambda_p) \\ \sin\theta_p \cos(\alpha_p + \lambda_p) \\ \sin(\alpha_p + \lambda_p) \end{bmatrix} \tag{21}$$

Equations of the Family of Generating Surface

The family of generating surfaces is represented in S_1 by the matrix equation

$$\begin{aligned} \mathbf{r}_1(\lambda_p, \theta_p, \psi_1) &= \mathbf{M}_{1a}(\psi_1)\mathbf{M}_{am}\mathbf{M}_{mc_1}(\psi_{c_1})\mathbf{M}_{c_1 t_1}\mathbf{r}_{t_1}(\lambda_p, \theta_p) \\ &= \mathbf{M}_{1t_1}(\psi_1)\mathbf{r}_{t_1}(\lambda_p, \theta_p) \end{aligned} \tag{22}$$

The product of matrices $\mathbf{M}_{1t_1}$ is based on the coordinate transformations from S_{t_1} to S_1 (figs. 5 and 8), where ψ_1 and ψ_{c_1} are related by equation (2). Here,

$$\mathbf{M}_{1a} = \begin{bmatrix} \cos\psi_1 & -\sin\psi_1 & 0 & 0 \\ \sin\psi_1 & \cos\psi_1 & 0 & 0 \\ 0 & 0 & 1 & 0 \\ 0 & 0 & 0 & 1 \end{bmatrix} \tag{23}$$

$$\mathbf{M}_{am} = \begin{bmatrix} -\sin\gamma_1 & 0 & -\cos\gamma_1 & 0 \\ 0 & 1 & 0 & 0 \\ \cos\gamma_1 & 0 & -\sin\gamma_1 & 0 \\ 0 & 0 & 0 & 1 \end{bmatrix} \tag{24}$$

$$\mathbf{M}_{mc_1} = \begin{bmatrix} \cos\psi_{c_1} & -\sin\psi_{c_1} & 0 & 0 \\ \sin\psi_{c_1} & \cos\psi_{c_1} & 0 & 0 \\ 0 & 0 & 1 & 0 \\ 0 & 0 & 0 & 1 \end{bmatrix} \tag{25}$$

$$\mathbf{M}_{c_1 t_1} = \begin{bmatrix} 1 & 0 & 0 & S_{r1}\cos q_1 \\ 0 & 1 & 0 & S_{r1}\sin q_1 \\ 0 & 0 & 1 & 0 \\ 0 & 0 & 0 & 1 \end{bmatrix} \tag{26}$$

Equation of Meshing

We derive the equation of meshing between the generating surface and pinion as

$$\mathbf{n}_{c_1} \cdot \mathbf{v}_{c_1}^{(c_1 1)} = f(\lambda_p, \theta_p, \psi_1) = 0 \tag{27}$$

where $\mathbf{v}_{c_1}^{(c_1 1)}$ is the relative velocity in the coordinate system S_{c_1}. The vectors are represented in S_{c_1}. Here,

$$\mathbf{v}_{c_1}^{(c_1 1)} = \omega_{c_1}^{(c_1 1)} \times \mathbf{r}_{c_1} = (\omega_{c_1}^{(c_1)} - \omega_{c_1}^{(1)}) \times \mathbf{r}_{c_1}^{(p)} \tag{28}$$

where

$$\begin{aligned} \mathbf{r}_{c_1} &= \mathbf{M}_{c_1 t_1}\mathbf{r}_{t_1} \\ &= \begin{bmatrix} R_1\cos(\alpha_p+\lambda_p)\cos\theta_p + B_1 \\ R_1\cos(\alpha_p+\lambda_p)\sin\theta_p + B_2 \\ -R_1(\sin\alpha_p - \sin(\alpha_p+\lambda_p)) \end{bmatrix} \end{aligned} \tag{29}$$

$$(\omega_{c_1}^{(c_1)} - \omega_{c_1}^{(1)}) = \begin{bmatrix} 0 \\ 0 \\ \omega_1\sin\gamma_1 \end{bmatrix} - \mathbf{L}_{c_1 m}\mathbf{L}_{ma}\mathbf{L}_{a1}\begin{bmatrix} 0 \\ 0 \\ -\omega_1 \end{bmatrix} = \begin{bmatrix} \omega_1\cos\gamma_1\cos\psi_{c_1} \\ -\omega_1\cos\gamma_1\sin\psi_{c_1} \\ 0 \end{bmatrix} \tag{30}$$

Using the designations

$$\left.\begin{aligned} B_1 &= R_p\cos\theta_p + S_{r1}\cos q_1 - R_1\cos\alpha_p\cos\theta_p \\ B_2 &= R_p\sin\theta_p + S_{r1}\sin q_1 - R_1\cos\alpha_p\sin\theta_p \end{aligned}\right\} \tag{31}$$

and considering that $|\omega_1| = 1$, we obtain from equation(28) that

$$\mathbf{v}_{c_1}^{(c_1 1)} = \begin{bmatrix} R_1(\sin\alpha_p - \sin(\alpha_p+\lambda_p))\cos\gamma_1\sin\psi_{c_1} \\ R_1(\sin\alpha_p - \sin(\alpha_p+\lambda_p))\cos\gamma_1\cos\psi_{c_1} \\ \cos\gamma_1(R_1\cos(\alpha_p+\lambda_p)\sin(\theta_p+\psi_{c_1}) + B_1\sin\psi_{c_1} + B_2\cos\psi_{c_1}) \end{bmatrix} \tag{32}$$

The equation of meshing (27) is represented as

$$\tan(\alpha_p + \lambda_p) = \frac{-R_1 \sin\alpha_p \sin(\theta_p + \psi_{c_1})}{B_1 \sin\psi_{c_1} + B_2 \cos\psi_{c_1}} \tag{33}$$

Equations of Pinion Tooth Surface

Equations (22) and (33) represent the pinion tooth surface by three related parameters. After elimination of parameter λ_p we may represent the pinion tooth surface by two independent parameters, θ_p and ψ_1.

$$\mathbf{r}_1 = \mathbf{r}_1(\theta_p, \psi_1) \tag{34}$$

5 Local Synthesis

The ideas of local synthesis are based on the following considerations [2]:

(1) The pinion and gear tooth surfaces are in tangency at the mean contact point M that is in the middle of the contacting surface.

(2) The gear ratio is equal to the theoretical one.

(3) We have to provide in the neighborhood of M the following transmission function (fig. 9)

$$\phi_2(\phi_1) = \frac{N_1}{N_2}\phi_1 - \frac{1}{2}m'_{21}\phi_1^2 \tag{35}$$

where $\frac{1}{2}m'_{21}$ is the parabola parameter of the predesigned parabolic function of transmission errors

$$\Delta\phi_2(\phi_1) = -\frac{1}{2}m'_{21}\phi_1^2 \tag{36}$$

(4) In addition it is necessary to provide the desired direction of the contact path.

All these goals can be achieved by the proper mismatch of the contacting surfaces of the pinion-gear tooth surfaces. The solution to this problem requires directions of the contacting surfaces. However, since the equations of the pinion and gear tooth surfaces are represented in a complex form, we will represent the principal curvatures and directions of the generated surfaces in terms of the principal curvatures and directions of the generating surfaces (the head-cutter surfaces) and the parameters of motion. The procedure of the local synthesis is as follows:

Step 1: We consider as given the surface of the head-cutter that generates the gear tooth surface. The head-cutter surface is a cone and is in line contact with the surface of the gear. One of such contact lines passes through the mean point M of tangency of the pinion and the gear tooth surfaces. Considering the surface of the gear head-cutter as known, we determine at point M the principal curvatures and directions of the gear head-cutter.

The principal directions of the generating cone are

$$\begin{aligned} \mathbf{e}_f^{(t_2)} &= \frac{\partial \mathbf{r}_{t_2}}{\partial \theta_g} \Big/ \left| \frac{\partial \mathbf{r}_{t_2}}{\partial \theta_g} \right| = [-\sin\theta_g \quad \cos\theta_g \quad 0]^T \\ \mathbf{e}_h^{(t_2)} &= \frac{\partial \mathbf{r}_{t_2}}{\partial s_g} \Big/ \left| \frac{\partial \mathbf{r}_{t_2}}{\partial s_g} \right| = [-\sin\alpha_g \cos\theta_g \quad -\sin\alpha_g \sin\theta_g \quad \cos\alpha_g]^T \end{aligned} \tag{37}$$

The principal curvatures of the generating cone are

$$\begin{aligned} k_f^{(t_2)} &= -\cos\alpha_g/(R_g - s_g \sin\alpha_g) \\ k_h^{(t_2)} &= 0 \end{aligned} \tag{38}$$

Step 2: Our next goal is to determine at M the principal curvature k_s and k_q and the principal directions of the gear tooth surface Σ_2. We apply for this purpose the equations that have been proposed in [2] and represent the direct relations between the principal curvatures and directions for two surfaces being in line contact.

Surface Σ_{t_2} and Σ_2 are in line contact when cone Σ_{t_2} generate the gear tooth surface Σ_2. The principal curvatures of the gear k_s and k_q can be obtained from the equations

$$\begin{aligned} \tan 2\sigma_g &= \frac{-2b_{13}b_{23}}{b_{23}^2 - b_{13}^2 - (k_f^{(t_2)} - k_h^{(t_2)})b_{33}} \\ k_q - k_s &= \frac{-2b_{13}b_{23}}{b_{33}\sin 2\sigma_g} \\ k_q + k_s &= k_f^{(t_2)} + k_h^{(t_2)} + \frac{b_{13}^2 + b_{23}^2}{b_{33}} \end{aligned} \tag{39}$$

where

$$\begin{aligned} b_{13} &= -k_f^{(t_2)} v_f^{(t_2 2)} + [\mathbf{n}\omega^{(t_2 2)}\mathbf{e}_f^{(t_2)}] \\ b_{23} &= -k_h^{(t_2)} v_h^{(t_2 2)} + [\mathbf{n}\omega^{(t_2 2)}\mathbf{e}_h^{(t_2)}] \\ b_{33} &= -k_f^{(t_2)}(v_f^{(t_2 2)})^2 - k_h^{(t_2)}(v_h^{(t_2 2)})^2 + [\mathbf{n}\omega^{(t_2 2)}\mathbf{v}^{(t_2 2)}] - \mathbf{n}\cdot[(\omega^{(t_2)} \times \mathbf{v}_{tr}^{(2)}) - (\omega^{(2)} \times \mathbf{v}_{tr}^{(t_2)})] \end{aligned} \tag{40}$$

The principal directions on the gear tooth surface are represented by unit vectors $\mathbf{e}_s$ and $\mathbf{e}_q$, where

$$\begin{bmatrix} \mathbf{e}_s \\ \mathbf{e}_q \end{bmatrix} = \begin{bmatrix} \cos\sigma_g & \sin\sigma_g \\ -\sin\sigma_g & \cos\sigma_g \end{bmatrix} \begin{bmatrix} \mathbf{e}_f^{(t_2)} \\ \mathbf{e}_h^{(t_2)} \end{bmatrix} \tag{41}$$

Step 3: We now consider that the gear and pinion tooth surfaces, Σ_2 and Σ_1, are in tangency at M. As a reminder, the mismatched gear and pinion tooth surfaces are in point contact at every instant.

Unit vectors $\mathbf{e}_s$ and $\mathbf{e}_q$ represent the known directions of the principal directions on surface Σ_2. The principal curvatures k_s and k_q on the gear principal directions are known. Our goal is to determine angle σ_{12} that is formed by vectors $\mathbf{e}_f$ and $\mathbf{e}_s$ (fig. 10) and the principal curvatures k_f and k_h of the pinion tooth surface at point M. Unit vectors $\mathbf{e}_f$ and $\mathbf{e}_h$ represent the sought-for principal directions on the pinion tooth surface Σ_1.

Step 4: The three unknowns: k_f, k_h and σ_{12} can be determined using the approach developed in [2]. We use for this purpose the following system of three linear equations. Three linear equations that related the velocity $\mathbf{v}_r^{(1)}$ of the contact point over surface Σ_1 are derived in reference [2] as:

$$\begin{array}{rcl} a_{11}v_s^{(1)} + a_{12}v_q^{(1)} & = & a_{13} \\ a_{12}v_s^{(1)} + a_{22}v_q^{(1)} & = & a_{23} \\ a_{13}v_s^{(1)} + a_{23}v_q^{(1)} & = & a_{33} \end{array} \tag{42}$$

The augmented matrix formed by the coefficients a_{i1}, a_{i2} and a_{i3} is a symmetric one [2]. Here, $v_s^{(1)}$ and $v_q^{(1)}$ are the components of the velocity of the contact point that moves in the process of meshing over the pinion tooth surfaces Σ_1. Coefficients a_{i1}, a_{i2} and a_{i3} are represented in terms of k_s, k_q, k_f, k_h, σ_{12} and the parameters of motion.

Step 5: Equation system (42) represents a system of three linear equations in two unknowns: $v_s^{(1)}$ and $v_q^{(1)}$. Surface Σ_1 and Σ_2 are in point contact, the path of contact has a definite direction, and the solution of equation system (42) with respect to $v_s^{(1)}$ and $v_q^{(1)}$ must be unique. Therefore, the rank of the augmented matrix formed by a_{i1}, a_{i2} and a_{i3} is equal to two. This yields that

$$\begin{vmatrix} a_{11} & a_{12} & a_{13} \\ a_{12} & a_{22} & a_{23} \\ a_{13} & a_{23} & a_{33} \end{vmatrix} = a_{11}a_{22}a_{33} + a_{12}a_{23}a_{13} + a_{13}a_{12}a_{23} - a_{22}a_{13}^2 - a_{11}a_{23}^2 - a_{33}a_{12}^2$$

$$= F(k_f,\ k_h,\ k_s,\ k_q,\ \sigma_{12},\ m'_{21}) = 0 \tag{43}$$

Here,

$$\begin{aligned}
a_{11} &= k_s - k_f \cos^2\sigma_{12} - k_h \sin^2\sigma_{12} \\
a_{12} &= 0.5(k_f - k_h)\sin 2\sigma_{12} \\
a_{13} &= -k_s v_s^{(12)} + [\mathbf{n}\omega^{(12)}\mathbf{e}_s] \\
a_{22} &= k_q - k_f \sin^2\sigma_{12} - k_h \cos^2\sigma_{12} \\
a_{23} &= -k_q v_q^{(12)} + [\mathbf{n}\omega^{(12)}\mathbf{e}_q] \\
a_{33} &= k_s(v_s^{(12)})^2 + k_q(v_q^{(12)})^2 - [\mathbf{n}\omega^{(12)}\mathbf{v}^{(12)}] \\
&\quad -\mathbf{n}\cdot[(\omega^{(1)} \times \mathbf{v}_{tr}^{(2)}) - (\omega^{(2)} \times \mathbf{v}_{tr}^{(1)})] + m'_{21}(\mathbf{n} \times \mathbf{k}_2)\cdot\mathbf{r}_m
\end{aligned} \tag{44}$$

$\sigma_{12} = \sigma_g - \sigma_p$ is the angle between the principal directions of this two contacting surface, m'_{21} is the derivative of $\phi_2(\phi_1)$ at the contact point. Coefficient a_{33} contains the derivative

$$m'_{21} = \frac{d}{d\phi_1}(m_{21}(\phi_1)) \tag{45}$$

where

$$m_{21} = \frac{d\phi_2}{d\phi_1} \tag{46}$$

From equation (43), we get

$$a_{33} = \frac{-a_{12}a_{23}a_{13} - a_{13}a_{12}a_{23} + a_{22}a_{13}^2 + a_{11}a_{23}^2}{a_{11}a_{22} - a_{12}^2} \tag{47}$$

Substituting equation (47) into equation (44), we can obtain the derivative

$$m'_{21} = \frac{a_{33} - k_s(v_s^{(12)})^2 - k_q(v_q^{(12)})^2 + [\mathbf{n}\omega^{(12)}\mathbf{v}^{(12)}] + \mathbf{n}\cdot[(\omega^{(1)} \times \mathbf{v}_{tr}^{(2)}) - (\omega^{(2)} \times \mathbf{v}_{tr}^{(1)})]}{(\mathbf{n} \times \mathbf{k}_2)\cdot\mathbf{r}_m} \tag{48}$$

The parabola coefficient of the parabolic function (36) is $m'_{21}/2$.

The other relation between the coefficients a_{i1}, a_{i2} and a_{i3} may be determined considering that

$$\tan\eta_1 = \frac{v_q^{(1)}}{v_s^{(1)}} \tag{49}$$

where η_1 is the assigned direction at M of the tangent to the path of contact on the pinion surface Σ_1.

Using the relations discussed above between the coefficients of linear equation [2], we are able to determine the sought-for pinion principal curvatures k_f, k_h and orientation angle σ_{12}.

Step 6: We consider now that for surface Σ_1 the followings are known: (i) the principal directions determined by unit vectors $\mathbf{e}_f$ and $\mathbf{e}_h$ (ii) the principal curvatures k_f and k_h, and (iii) angle σ_{12} formed by unit vectors $\mathbf{e}_f$ and $\mathbf{e}_s$ (fig. 10). Our goal is to determine the principal curvatures and directions of the pinion head-cutter generating surface that is designed as the surface of revolution (fig. 3). The pinion head-cutter surface and the pinion tooth surface are in line contact at every instant. Using the direct relations between the principal curvatures and directions for two surfaces being in line contact [2], we may determine the principal curvatures and principal directions of the pinion head-cutter. Then, the desired mismatch of the surfaces of the gear and the pinion will be provided by the generation of the gear and the pinion by the designed head-cutters.

Using the approach discussed above, we obtain the following equations

$$\begin{aligned}
\tan 2\sigma_p &= \frac{-2b'_{13}b'_{23}}{b'^2_{23} - b'^2_{13} - (k_s^{(t_1)} - k_q^{(t_1)})b'_{33}} \\
k_h - k_f &= \frac{-2b'_{13}b'_{23}}{b'_{33}\sin 2\sigma_p} \\
k_h + k_f &= k_s^{(t_1)} + k_q^{(t_1)} + \frac{b'^2_{13} + b'^2_{23}}{b'_{33}}
\end{aligned} \tag{50}$$

where

$$\begin{aligned}
b'_{13} &= -k_s^{(t_1)} v_s^{(t_1 1)} + [\mathbf{n}\omega^{(t_1 1)}\mathbf{e}_s^{(t_1)}] \\
b'_{23} &= -k_q^{(t_1)} v_q^{(t_1 1)} + [\mathbf{n}\omega^{(t_1 1)}\mathbf{e}_q^{(t_1)}] \\
b'_{33} &= -k_s^{(t_1)}(v_s^{(t_1 1)})^2 - k_q^{(t_1)}(v_q^{(t_1 1)})^2 + [\mathbf{n}\omega^{(t_1 1)}\mathbf{v}^{(t_1 1)}] - \mathbf{n}\cdot[(\omega^{(t_1)} \times \mathbf{v}_{tr}^{(1)}) - (\omega^{(1)} \times \mathbf{v}_{tr}^{(t_1)})]
\end{aligned} \tag{51}$$

The principal directions on the pinion and the pinion head-cutter are related as follows

$$\begin{bmatrix} \mathbf{e}_f \\ \mathbf{e}_h \end{bmatrix} = \begin{bmatrix} \cos\sigma_p & \sin\sigma_p \\ -\sin\sigma_p & \cos\sigma_p \end{bmatrix} \begin{bmatrix} \mathbf{e}_s^{(t_1)} \\ \mathbf{e}_q^{(t_1)} \end{bmatrix} \tag{52}$$

where the principal directions of the generating surface of revolution are

$$\mathbf{e}_s^{(t_1)} = \frac{\partial \mathbf{r}_{t_1}}{\partial \theta_p} \Big/ \left|\frac{\partial \mathbf{r}_{t_1}}{\partial \theta_p}\right| = [-\sin\theta_p \quad \cos\theta_p \quad 0]^T$$

$$\mathbf{e}_q^{(t_1)} = \frac{\partial \mathbf{r}_{t_1}}{\partial \lambda_p} \Big/ \left|\frac{\partial \mathbf{r}_{t_1}}{\partial \lambda_p}\right| = [-\sin(\alpha_p+\lambda_p)\cos\theta_p \quad -\sin(\alpha_p+\lambda_p)\sin\theta_p \quad \cos(\alpha_p+\lambda_p)]^T \tag{53}$$

The principal curvatures of the generating surface of revolution are

$$\begin{aligned} k_s^{(t_1)} &= -\cos(\alpha_p+\lambda_p)/(R_p + R_1(\cos(\alpha_p+\lambda_p) - \cos\alpha_p)) \\ k_q^{(t_1)} &= -1/R_1 \end{aligned} \tag{54}$$

Equations (53) and (54) permit the representation of the principal curvatures and directions on the pinion head-cutter surface in terms of R_1 and R_p. We remind that equations (48) and (49) contain parameters R_1 and R_p (figs. 2). Considering as given m'_{21} and η_1, we can determine from equation (48) and (49) R_1 and R_p.

Step 7: At this step we know the principal curvatures and directions on the pinion and the gear, and the principal curvatures and directions on the pinion and gear head-cutters. The obtained mismatch of pinion and gear tooth surfaces will provide in the neighborhood of the mean contact point the desired parabolic function of transmission errors and the direction of the contact path. The principal curvatures and directions obtained on the pinion and gear head-cutters will provide the required mismatch of the pinion and gear tooth surface. Our next goal is to determine the dimensions of the instantaneous contact ellipse and its orientation, considering as given the elastic approach of the contacting surfaces.The solution is based on the following procedure [2].

The major axis and minor axis of the contact ellipse can be determined as

$$2a = 2\sqrt{\left|\frac{\delta}{A}\right|}, \quad 2b = 2\sqrt{\left|\frac{\delta}{B}\right|} \tag{55}$$

where δ is the elastic approach obtained from experimental data; A and B are determined

by

$$\begin{aligned} A &= \tfrac{1}{4}[k_\Sigma^{(1)} - k_\Sigma^{(2)} - (g_1^2 - 2g_1g_2\cos 2\sigma_{12} + g_2^2)^{\frac{1}{2}}] \\ B &= \tfrac{1}{4}[k_\Sigma^{(1)} - k_\Sigma^{(2)} + (g_1^2 - 2g_1g_2\cos 2\sigma_{12} + g_2^2)^{\frac{1}{2}}] \end{aligned} \tag{56}$$

and

$$\begin{aligned} k_\Sigma^{(1)} &= k_f + k_h \qquad & k_\Sigma^{(2)} &= k_s + k_q \\ g_1 &= k_f - k_h \qquad & g_2 &= k_s - k_q \end{aligned} \tag{57}$$

The orientation of the contact ellipse in the tangent plane is determined by

$$\cos 2\alpha = \frac{g_1 - g_2\cos\sigma_{12}}{(g_1^2 - 2g_1g_2\cos 2\sigma_{12} + g_2^2)^{\frac{1}{2}}} \tag{58}$$

Directions for the Computational Procedure of Local Synthesis

Step 1: The parameters of the gear head-cutter and its installment are considered as known (see, for instance, Table 2).

Step 2: The mean contact point is considered as known as well (It is determined by the application of the TCA program that provides the tangency of contacting surfaces at the mean contact point).

Step 3: Using equations (39) and (41), we determine at the mean contact point the principal curvatures (k_s, k_q) and the principal directions represented by unit vectors $\mathbf{e}_s$ and $\mathbf{e}_q$ (fig. 10).

Step 4: We use the values R_1 and R_p (fig. 3) as the first guess for the pinion head cutter. Then, we determine at the mean contact point the principal curvatures $k_s^{(t_1)}$, $k_q^{(t_1)}$, and principal directions represented by $\mathbf{e}_s^{(t_1)}$, $\mathbf{e}_q^{(t_1)}$ applying for this purpose equation (53) and (54).

Step 5: We compute the principal curvatures k_f, k_h of the pinion tooth surface and principal directions represented by unit vectors $\mathbf{e}_f$ and $\mathbf{e}_h$ applying for this purpose equations (50) and (52).

Step 6: Choosing m'_{21} and η_1 and then applying equations (48) and (49), we determine the final values of R_1 and R_p. The process of computation is an iterative one and requires for the solution a first guess of parameters R_1 and R_p.

6 Tooth Contact Analysis

The purpose of TCA is to determine the influence of misalignment on the shift of the bearing contact and the transmission errors. This goal is to be obtained by simulation of meshing and contact of the pinion and gear tooth surfaces of a misaligned gear drive.

We consider that the pinion and gear tooth surfaces are analytically represented in coordinate systems S_1 and S_2 (see sections 3 and 4, respectively). The meshing of pinion and gear tooth surfaces is considered in fixed coordinate system S_h (figs. 11 and 12). Auxiliary fixed coordinate system S_a and S_e are applied to describe the installment of the pinion with respect to S_h (fig. 11). The pinion alignment error ΔA_p is the pinion axial displacement. The misaligned pinion in the process of meshing with the gear performs rotation about Z_e-axis. The current angle of rotation of the pinion is designated by ϕ_1 (fig. 11).

Auxiliary coordinate systems S_b, S_c and S_d are applied to describe the installment of misaligned gear with respect to S_h. The errors of alignment are: the change $\Delta\gamma$ of the shaft angle (fig. 12), the offset ΔE and the gear axial displacement ΔA_g (fig. 13). The misaligned gear performs rotation about the Z_d-axis, and ϕ_2 is the current angle of the gear rotation.

A TCA computer program was developed to simulate the meshing of pinion-gear tooth surfaces of the misaligned gear drive. The development of the TCA program is based on the following ideas:

Step 1: We consider that the pinion and gear tooth surfaces and the surface unit normals are represented in coordinate system S_1 and S_2 by vector functions

$$\mathbf{r}_1(\theta_p, \psi_1) \text{ and } \mathbf{r}_2(\theta_g, \psi_2) \tag{59}$$

$$\mathbf{n}_1(\theta_p, \psi_1) \text{ and } \mathbf{n}_2(\theta_g, \psi_2) \tag{60}$$

where (θ_p, ψ_1) and (θ_g, ψ_2) are the surface parameters.

Step 2: We represent now the pinion-gear tooth surfaces and their surface unit normals in coordinate system S_h, and take into account that the surfaces are in continuous tangency.

Then we obtain the following equations

$$\mathbf{r}_h^{(1)}(\theta_p, \psi_1, \phi_1) - \mathbf{r}_h^{(2)}(\theta_g, \psi_2, \phi_2) = 0 \tag{61}$$

$$\mathbf{n}_h^{(1)}(\theta_p, \psi_1, \phi_1) - \mathbf{n}_h^{(2)}(\theta_g, \psi_2, \phi_2) = 0 \tag{62}$$

where

$$\mathbf{r}_h^{(1)}(\theta_p, \psi_1, \phi_1) = \mathbf{M}_{h1}(\phi_1)\mathbf{r}_1(\theta_p, \psi_1) \tag{63}$$

$$\mathbf{r}_h^{(2)}(\theta_g, \psi_2, \phi_2) = \mathbf{M}_{h2}(\phi_2)\mathbf{r}_2(\theta_g, \psi_2) \tag{64}$$

$$\mathbf{n}_h^{(1)}(\theta_p, \psi_1, \phi_1) = \mathbf{L}_{h1}(\phi_1)\mathbf{n}_1(\theta_p, \psi_1) \tag{65}$$

$$\mathbf{n}_h^{(2)}(\theta_g, \psi_2, \phi_2) = \mathbf{L}_{h2}(\phi_2)\mathbf{n}_2(\theta_g, \psi_2) \tag{66}$$

$$\mathbf{M}_{h1}(\phi_1) = \begin{bmatrix} \cos\phi_1 & \sin\phi_1 & 0 & 0 \\ -\sin\phi_1 & \cos\phi_1 & 0 & 0 \\ 0 & 0 & 1 & \Delta A_p \\ 0 & 0 & 0 & 1 \end{bmatrix} \tag{67}$$

$$\begin{aligned} \mathbf{M}_{h2}(\phi_2) &= \mathbf{M}_{hb}\mathbf{M}_{b2} \\ &= \begin{bmatrix} -\sin\Delta\gamma & 0 & -\cos\Delta\gamma & 0 \\ 0 & 1 & 0 & \Delta E \\ \cos\Delta\gamma & 0 & -\sin\Delta\gamma & 0 \\ 0 & 0 & 0 & 1 \end{bmatrix} \begin{bmatrix} \cos\phi_2 & -\sin\phi_2 & 0 & 0 \\ \sin\phi_2 & \cos\phi_2 & 0 & 0 \\ 0 & 0 & 1 & \Delta A_g \\ 0 & 0 & 0 & 1 \end{bmatrix} \end{aligned} \tag{68}$$

Equations (61) and (62) represent the conditions that the contacting surfaces at the point of tangency have a common position vector and a common surface unit normal. Equations (61) and (62) yield a system of five independent scalar equations of the following structure

$$f_i(\theta_p, \psi_1, \phi_1, \theta_g, \psi_2, \phi_2) = 0 \qquad f_i \in C^1 \qquad (i = 1..5) \tag{69}$$

As a reminder, vector equation (62) yields only two independent scalar equations, and not three, since $|\mathbf{n}_h^{(1)}| = |\mathbf{n}_h^{(2)}| = 1$.

Step 3: System (69) of five nonlinear equations contains six unknowns, but one of the unknowns, say ϕ_1, may be considered as the input parameter. Our goal is the numerical solution of nonlinear equations (69) by functions

$$\{\theta_p(\phi_1), \psi_1(\phi_1), \theta_g(\phi_1), \psi_2(\phi_1), \phi_2(\phi_1)\} \in C^1 \tag{70}$$

The sought-for numerical solution is an iterative process that requires on each iteration the observation of the following conditions [2, 4, 5, 11]:

(i) There is a set of parameters (the first guess)

$$P(\theta_p^{(o)}, \psi_1^{(o)}, \phi_1^{(o)}, \theta_g^{(o)}, \psi_2^{(o)}, \phi_2^{(o)}) \tag{71}$$

that satisfies the equation system (69).

(ii) The Jacobian taken at P differs from zero. Thus, we have

$$\Delta_5 = \frac{D(f_1, f_2, f_3, f_4, f_5)}{D(\theta_p, \psi_1, \theta_g, \psi_2, \phi_2)} \neq 0 \tag{72}$$

Then, as it follows from the Theorem of Implicit Function System Existence, equation system (69) can be solved in the neighborhood of P by functions (70).

Using the obtained solution, we can determine the path of contact on the pinion-gear tooth surface, and the transmission errors caused by misalignment. The path of contact on surface Σ_i $(i = 1, 2)$ is determined by the expressions

$$\mathbf{r}_1(\theta_p, \psi_1), \quad \theta_p(\phi_1), \quad \psi_1(\phi_1) \tag{73}$$

$$\mathbf{r}_2(\theta_g, \psi_2), \quad \theta_g(\phi_1), \quad \psi_2(\phi_1) \tag{74}$$

The transmission errors are determined by the equation

$$\Delta\phi_2 = \phi_2(\phi_1) - \frac{N_1}{N_2}\phi_1 \tag{75}$$

The dimensions and orientation of the instantaneous contact ellipse at the contact point may be determined considering that the principal curvatures and directions of the contacting surfaces, and the elastic approach of the surface [2] are known (see step 7 in section 5).

7 Avoidance of Pinion Undercutting

In most cases undercutting can be avoided, if the appearance of singular points on the generated surface is avoided. Singularities on the surface occur when the normal to the surface becomes equal to zero. To avoid undercutting of the pinion by the generating tool, the approach developed in [7, 8, 9] is applied:

Step 1: Consider that the surface of the generating tool is represented as

$$\mathbf{r}_{t_1} = \mathbf{r}_{t_1}(\lambda_p, \theta_p) \tag{76}$$

The equation of meshing is represented as

$$f_1(\lambda_p, \theta_p, \psi_1) = 0 \tag{77}$$

Step 2: It is proven in [7, 8, 9] that singular points occur if

$$\mathbf{v}_r^{(t_1)} + \mathbf{v}^{(t_1 1)} = 0 \tag{78}$$

where $\mathbf{v}_r^{(t_1)}$ is the velocity of the contact point in its motion over the tool surface, and $\mathbf{v}^{(t_1 1)}$ is the relative velocity. This yields that a matrix

$$A = \begin{vmatrix} \dfrac{\partial \mathbf{r}_{t_1}}{\partial \lambda_p} & \dfrac{\partial \mathbf{r}_{t_1}}{\partial \theta_p} & -\mathbf{v}_{t_1}^{(t_1 1)} \\ \dfrac{\partial f_1}{\partial \lambda_p} & \dfrac{\partial f_1}{\partial \theta_p} & -\dfrac{\partial f_1}{\partial \psi_1}\dfrac{\partial \psi_1}{\partial t} \end{vmatrix} \tag{79}$$

has the rank $r = 2$ and therefore three determinants Δ_i $(i = 1, 2, 3)$ of the third order must be equal to zero. Then we obtain that

$$F_1(\lambda_p, \theta_p, \psi_1) = \Delta_1^2 + \Delta_2^2 + \Delta_3^2 = 0 \tag{80}$$

Equations (77) and (80) permit the function $\lambda_p(\theta_p)$ to be determined for the limiting line on the tool surface. Then, we are able to determine the limiting line on the generating surface by the equation

$$\mathbf{r}_{t_1} = \mathbf{r}_{t_1}(\theta_p, \lambda_p(\theta_p)) \tag{81}$$

Fig. 14 shows the limiting line on the pinion tool surface.

Step 3: Using coordinate transformation, we may determine the line of singular points on the pinion tooth surface. (fig. 15)

Step 4: To avoid undercutting, we have to limit the dimension of the dedendum of the pinion tooth.

Fig. 16 shows the axial section of the pinion head-cutter. Parameter h represents the distance of a point of the axial section from the reference circle determined as

$$R_1 \sin \alpha_p - R_1 \sin(\alpha_p + \lambda_p) = h \tag{82}$$

To verify that undercutting has been avoided the following inequality must be observed

$$R_1[\sin \alpha_p - \sin(\alpha_p + \lambda_p(\theta_p))] > h_d \tag{83}$$

where h_d is the dedendum height of the pinion, and $\lambda_p(\theta_p)$ represents the function that corresponds to the points of the limiting line.

The design of spiral bevel gears is based on application of special tooth element proportions for the avoidance of undercutting: small pinion dedendums and long pinion addendums.

8 Numerical Example

As a numerical example the blank data is given in Table 1.

The gear head-cutter is a cone (figs. 2, 3 and 4), the cutter radius is designated by R_g (fig. 1), the radial setting of the head-cutter is $\left|\overline{O_{c_2}O_{t_2}}\right|$ (fig. 5(b)), and the installment angle is q_2 (fig. 5). The data for the gear head-cutter that generates the gear concave side are presented in Table 2.

The parameters of the pinion head-cutter were determined by application of the method of the local synthesis (section 5). The data for the pinion head-cutter that generates the pinion convex side are represented in Table 3. We considered in the numerical examples the meshing of the gear tooth concave side with the pinion tooth convex side. Case 1 corresponds to the orientation of the bearing contact across the surface, case 2 corresponds to the orientation of the bearing contact in the longitudinal direction.

The application of TCA for the simulation of meshing and contact permits the determination of misalignment effects on the transmission errors and the shift of the bearing contact. It has been shown that in the case of application of ideal generating surfaces (without mismatch, figs. 1 and 2) the errors of misalignment cause indeed discontinuous almost linear transmission errors as shown in fig. 17 for shaft angle error $\Delta\gamma$. Similar functions of transmission errors are caused by errors ΔA_p, ΔA_g and ΔE. Table 4 shows the maximum transmission errors caused by misalignment.

The results of TCA for the properly mismatched generating surfaces (see section 5) confirmed that a predesigned parabolic function indeed absorbs the transmission errors caused by misalignment, and the resulting function of transmission is a parabolic one (fig. 18). The absorption of linear function of transmission errors is carried out as well in other cases of misalignment: ΔA_p, ΔA_g and ΔE. The bearing contact of the drive is stable, and its shift is permissible (fig. 19). Model 2 of the gear drive (with longitudinal direction of the bearing contact) is preferable due to the lower level of transmission errors caused by misalignment.

9 Conclusion

From the conducted study the following general conclusions can be drawn:

(1) An approach has been developed for the synthesis of spiral bevel gears that provides (i) localized bearing contact, and (ii) low level of transmission errors of a parabolic type. The developed approach permits two possible directions of the bearing contact: across the tooth surface or in the longitudinal direction.

(2) A Tooth Contact Analysis (TCA) computer program for the investigation of the influence of misalignment on the shift of the bearing contact was developed.

(3) A low level of transmission errors, the parabolic type of the function of transmission errors, and the localization of the bearing contact are achieved by the proper mismatch of contacting surfaces.

(4) The influence of the following errors of alignment was investigated: (i) for axial displacement of the pinion, (ii) axial displacement of the gear, (iii) offset, and (iv) change of the shaft angle. These types of misalignment were proven to cause discontinuous almost linear functions of transmission errors, but they are absorbed by the predesigned parabolic function of transmission errors.

(5) Conditions of nonundercutting of the pinion were determined.

The results of this investigation show that a predesigned parabolic function can indeed absorb the linear functions of transmission errors caused by misalignment. The design of gears with a longitudinal bearing contact (in comparison with the bearing contact across the surface) is preferable since a lower level of transmission errors can be obtained.

10 Manual for Computer Program

Program Names and Purpose of the Programs

There are three programs

1. Program for Local Synthesis: *Localsyn.for*
2. Program for TCA: *Tca.for*
3. Program for Undercutting: *Undercut.for*

These programs are directed at the synthesis of the spiral bevel gear with uniform tooth height by using mismatched generating surfaces. The programs cover the local synthesis, tooth contact analysis and nonundercutting conditions. Using the programs, one can obtain the tooth surfaces, the contact lines on the tooth surface, the contact path on the tooth surface, the transmission errors and the bearing contact caused by misalignment of the gear drive, and the limiting lines on the generating tool surface and the pinion tooth surface.

Environment for Running the Programs

These programs were developed by application on an IBM PC and can be run using the software "Power Fortran".

An application of the subroutine HYBRD1 [11] for solving a system of nonlinear equations and several other subroutines that was called by HYBRD1 are required and included.

Input Data

1. Blank data

TN1—Pinion number of teeth

TN2—Gear number of teeth

TW—Face width of gear (mm)

GAMA—Shaft angle (degree)

Beta1—Pinion spiral angle (degree)

Beta2—Gear spiral angle (degree)

EllipseDelta—Elastic approach (mm)

2. Gear cutter specification

RU2—Gear nominal cutter radius (mm)

PW2—Point width of gear cutter (mm)

AFA_g—Blade angle of gear cutter (degree)

Rg—Cutter radius (mm)

3. Gear machine-tool settings

GAMA2—Gear machine pitch angle (degree)

Sr2—Radial setting (mm)

q2—Installment angle (degree)

4. Pinion machine-tool settings

GAMA1—Pinion machine pitch angle (degree)

Sr1—Radial setting (mm)

q1—Installment angle (degree)

5. Pinion cutter specification

Rp—Cutter radius (mm)

R1— Radius of surface of revolution(mm)

AFA_p—Profile angle of gear cutter (degree)

6. Misalignments

H—Axial displacement of the pinion (mm)

Q—Axial displacement of the gear (mm)

V—Offset displacement (mm)

Delta—Change of shaft angle (arc min.)

7. Local synthesis

Eta1— Tangent to the contact path on pinion surface at the mean contact point(degree)

plantm21— Coefficient of the parabolic function

Output data files

File *phi1phi2.k1:* Transmission errors $\Delta\phi_2$

File *sgthetag.k1:* Contact line on gear generating surface

File *spthetap.k1:* Contact line on pinion generating surface

File *contactp.k1*: Contact path on pinion tooth surface

File *contactg.k1*: Contact path on gear tooth surface

File *ellipse.k1*: Bearing contact on the pinion surface

File undercut.*k1*: The limiting line on pinion tooth surface (for avoidance of undercutting)

Procedure of using the programs

Step 1: Run program *Tca.for* for the condition of no misalignment by supplying the first

guess of R1 and Rp.

Step 2: In the output file contactg.*k1* we will get from the first line the x, y and z coordinates of the first contact point.

Step 3: Run program *Localsyn.for* for the desired plantm21 and eta1. Then we can get R1 and Rp.

Step 4: Check if R1 and Rp at Step 1 and Step 4 are the same or not. If both are the same then go to Step 6.

Step 5: Use the new values that we got from Step 4, recalculate the first contact point by running program *Tca.for*, and go to Step 3.

Step 6: Run program *Tca.for* with misalignment to obtain the transmission errors in the output file phi1phi2.*k1*.

Step 7: Run the program *Undercut.for* to check up the undercutting in the output file underp.*k1*.

11 References

(1) Litvin, F.L. Pahman P. and Goldrich R.N. 1982, "Mathematical Models for the Synthesis and Optimization of Spiral Bevel Gear Tooth Surfaces", NASA CR-3553

(2) Litvin, F.L. 1994, *Gear Geometry and Applied Theory*, Prentice Hall

(3) Litvin, F. L. and Zhao, X. 1996, "Computerized Design and Analysis of Face-milled, Uniform Tooth Height, Low-Noise Spiral Bevel Gear Drives", NASA Contractor Report 4704.

(4) Korn, G.A. and Korn, T.M. 1968, *Mathematics Handbook for Scientists and Engineers*, 2nd ed., McGraw-Hill, NY.

(5) Dongarrd, J.J., Bunch, J.R., Moler, C.B., and Steward, G.W. 1979, *LINPACK User's Guide*, SIAM, Philadelphia

(6) Favard, J. Course of Local Differential Geometry, Gauthier-Villars, Paris (in French, translated into Russian)

(7) Litvin, F.L. 1960, 1968, *Theory of Gearing*, 1st ed. (1960), 2nd ed. (1968). Nauka (in Russian)

(8) Litvin, F.L. 1969, "Die Beziehungen Zwischen den Krümmungen der Zahnoberflächen bei Räumlichen Verzahnungen". Z. Angew. *Math. Mech.* 49: 685-690 (in German)

(9) Litvin, F.L. and Zhang, Y. 1991, "Local Synthesis and Tooth Contact Analysis of Face-Milled Spiral Bevel Gears". NASA Contractor Report 4342, AVSCOM Technical Report 90-C-028

(10) Litvin, F.L. 1989, *Theory of Gearing*, NASA Reference Publication 1212

(11) More, Jorge J., Garbow, Burton S., and Hilstorm, Kenneth E. 1980, *User Guide for MINPACK-1*, Argonne National Laboratory, Argonne, IL.

(12) Stadtfeld, H.J. 1993, *Handbook of Bevel and Hypoid Gears,* Rochester Institute of Technology

(13) Zalgaller, V.A. 1975, *Theory of Envelopes*, Nauka, Moscow (in Russian)

Table 1: Blank Data

	Pinion	Gear
N_1,N_2, Number of teeth	11	41
γ, Shaft angle	90°	
Mean spiral angle	35°	35°
Hand of spiral	RH	LH
Whole depth (mm)	6.5	6.5
Tooth module (mm)	4.33	
Face width (mm)	27.25	27.25
γ_1, γ_2, Pitch angles	15°1′	74°59′

Table 2: Parameters and Installment of Gear Head-Cutter on gear concave side

α_g, Blade angle	20°
R_g, Cutter radius at mean point (mm)	78.52
S_{r2}, Radial setting (mm)	70.53
q_2, Installment angle	−62°14′

Table 3: Parameters and Installment of the Pinion Head-Cutter on pinion convex side

	Case 1	Case 2
α_p, Profile angle	20°	20°
INPUT		
η_1, Tangent direction of the contact path	171°	92°
m'_{21}, Derivative of $\phi_2(\phi_1)$	-1.3e-3	-1.2e-3
$\Delta\phi_2$=$0.5m'_{21}(\pi/N_1)^2$, Theoretical Max. (")	-10.94	-10.09
OUTPUT		
M, Mean contact point in S_m (mm)	(79.88, 0.39, 0.17)	(77.83, 1.64, 0.72)
R_p, Cutter radius at mean point (mm)	78.0	64.7
R_1, Radius of the surface of revolution (mm)	235.0	765.0
S_{r1} (mm)	70.30	65.38
q_1, Installment angle	−61°51′	−51°24′
Length of major axis of contact ellipse (mm)	12.54	4.5

Table 4: Maximum Transmission Errors for Generating Surfaces with Mismatch

	$\Delta\phi_2$ *in arc sec.*	
	Case 1	Case 2
$\Delta A_p = 0.1mm$	8.8	16.2
$\Delta A_g = 0.1mm$	11.5	12.5
$\Delta E = 0.1mm$	11	15
$\Delta\gamma = 3'$	10.7	13.5

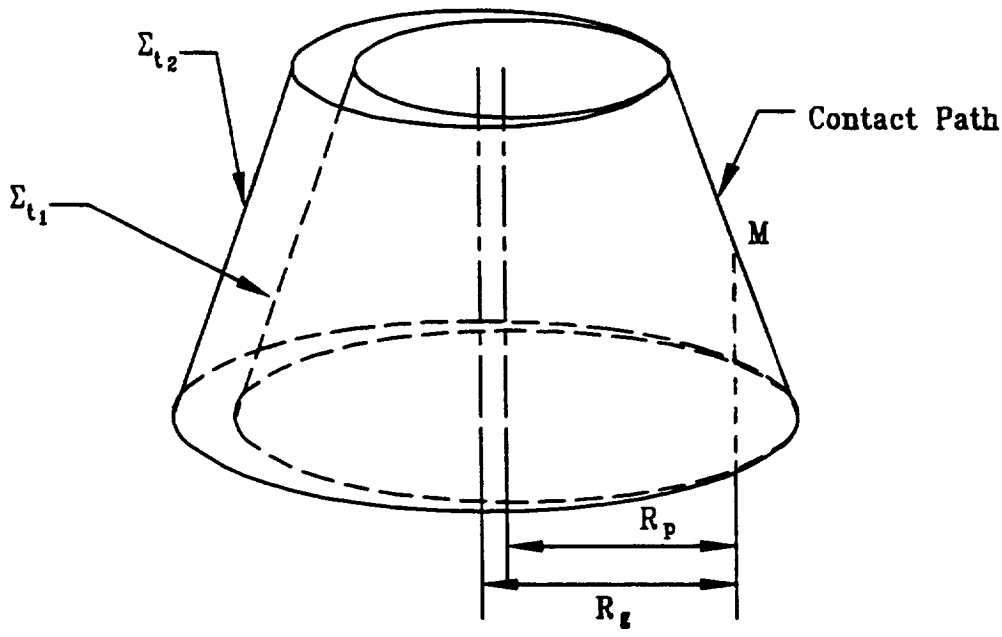

Fig. 1: Generating cones

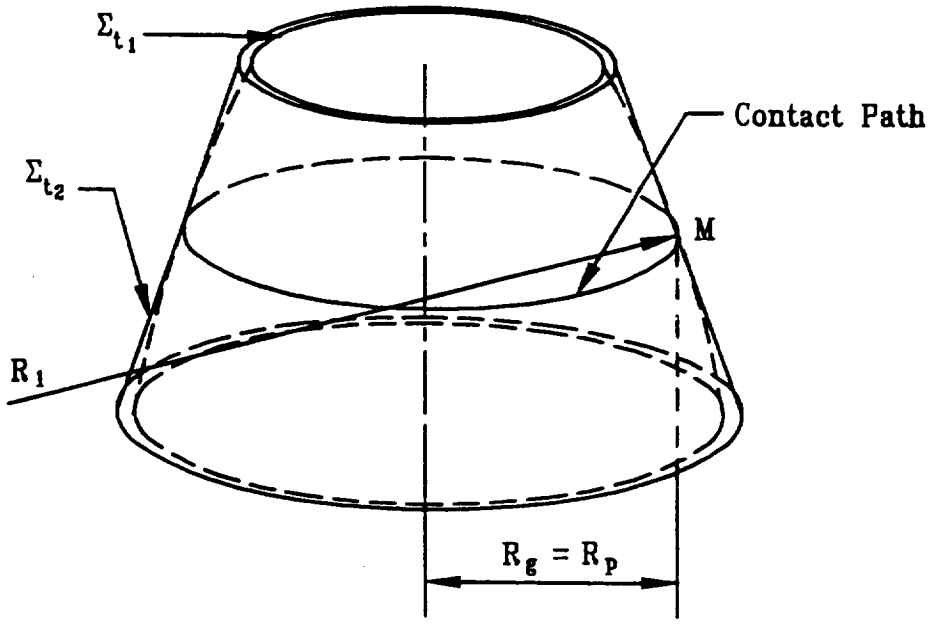

Fig. 2: Generating cone and generating surface of revolution

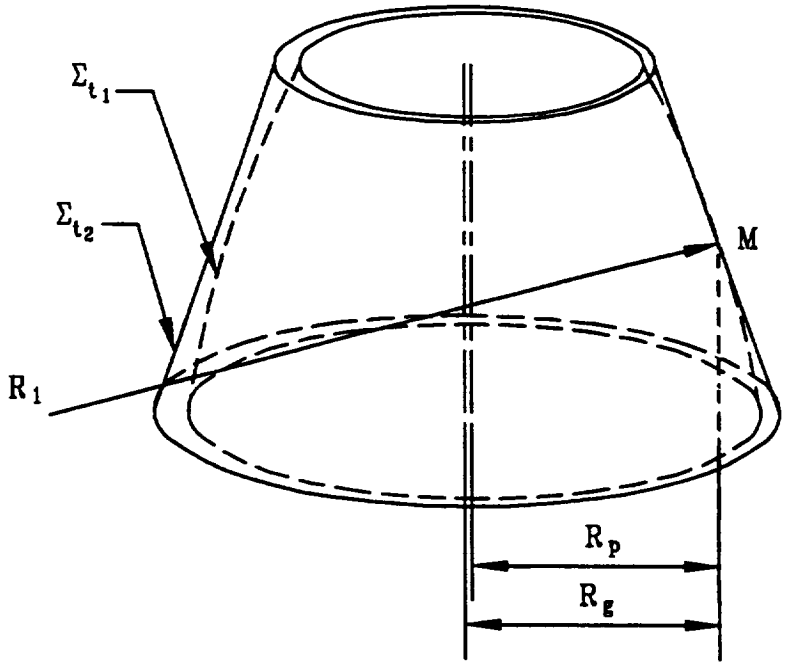

Fig. 3: Mismatched generating surfaces

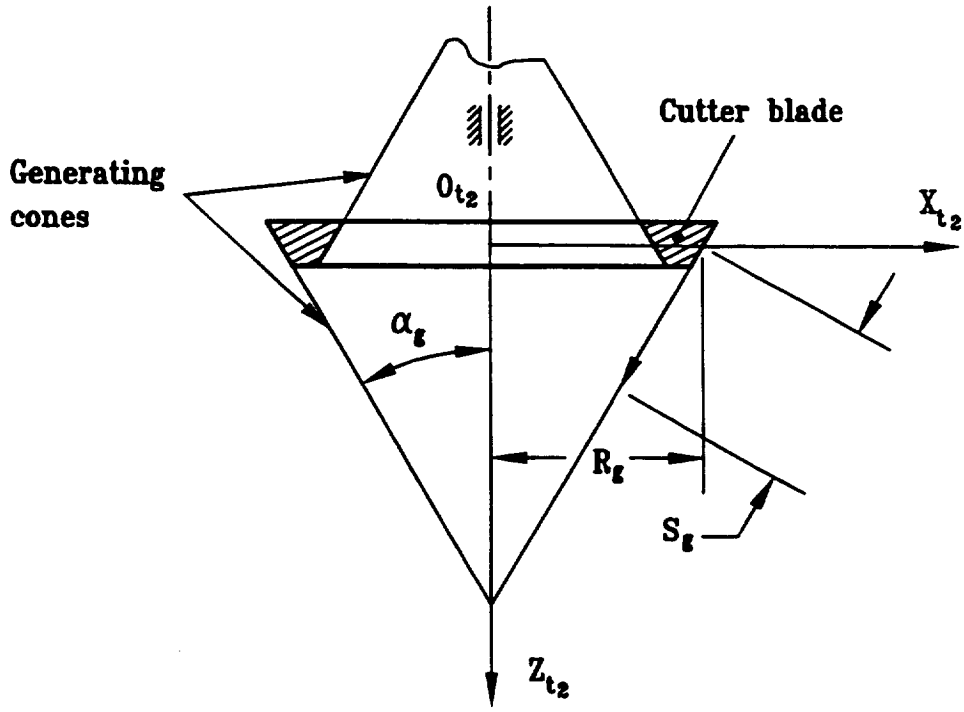

Fig. 4: Cones for gear generation

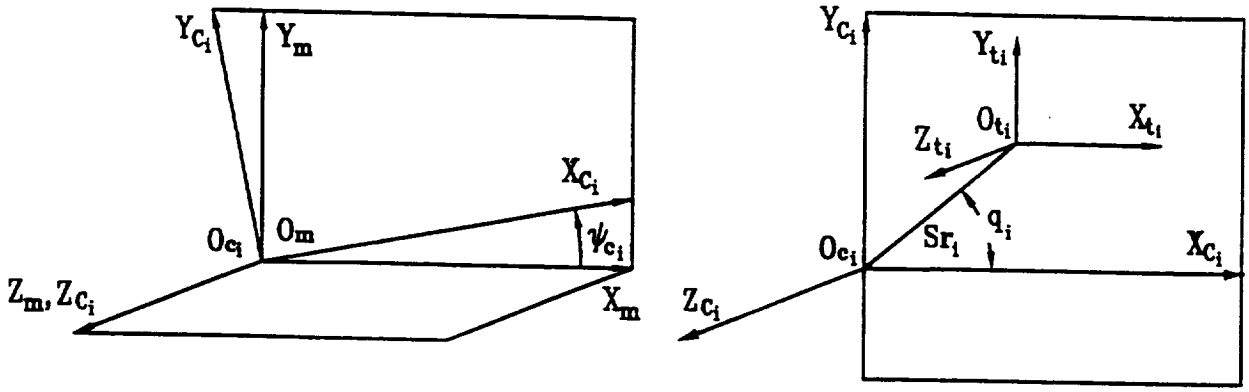

(a) (b)

Fig. 5: Coordinate systems S_c and S_m

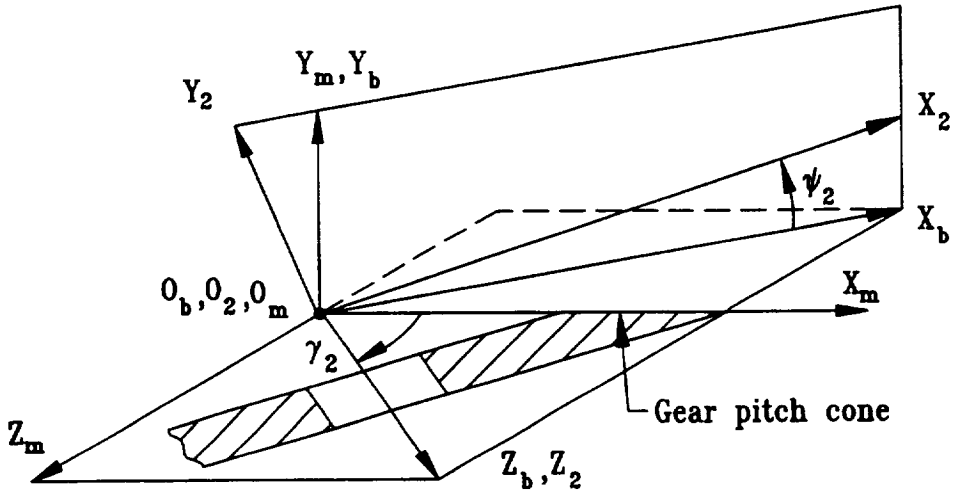

Fig. 6: Coordinate systems S_m, S_b and S_2

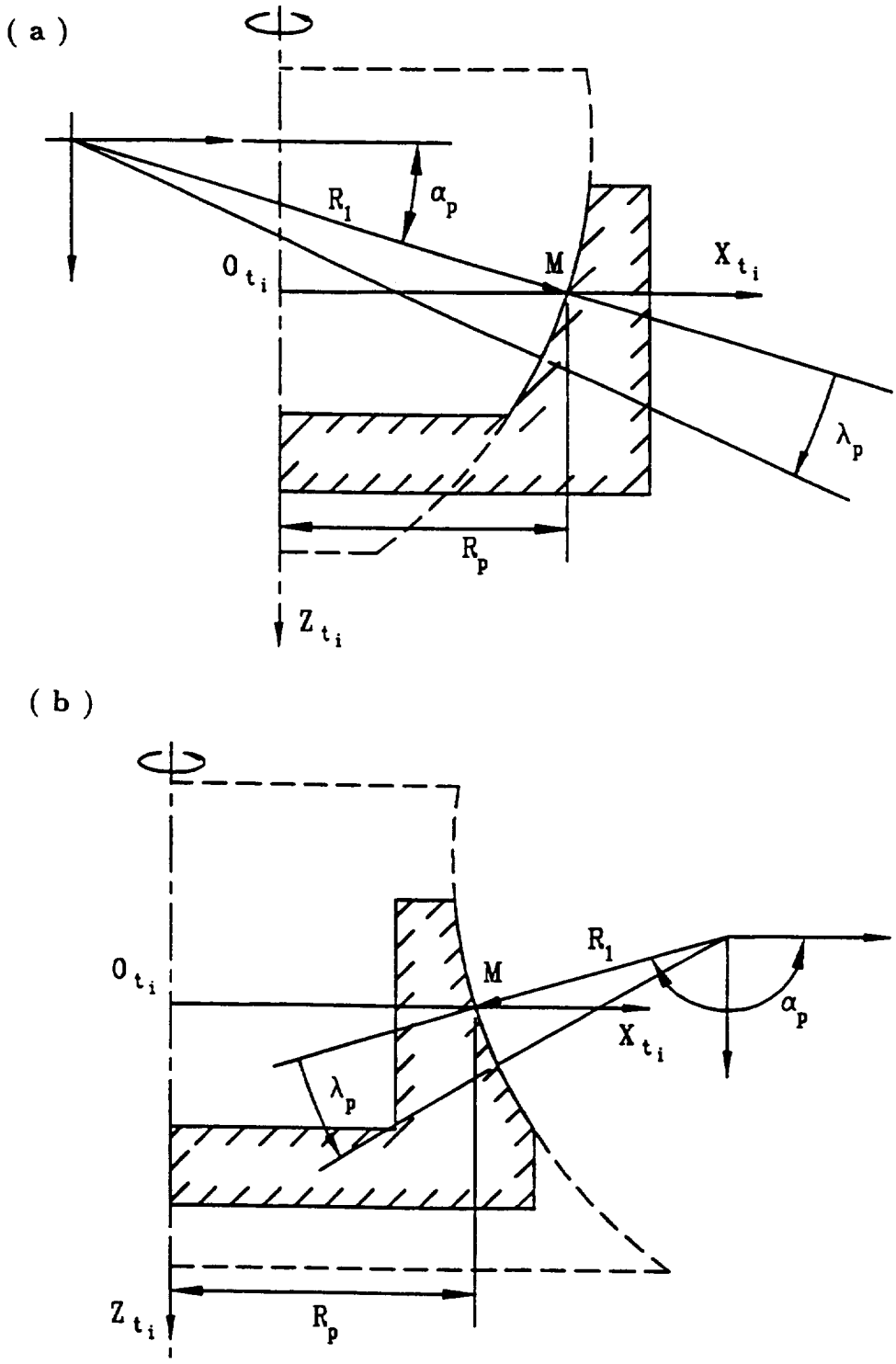

Fig. 7: (a)Convex (Inside blade) and (b)concave (outside blade) sides of the generating blades and generating surfaces of revolution

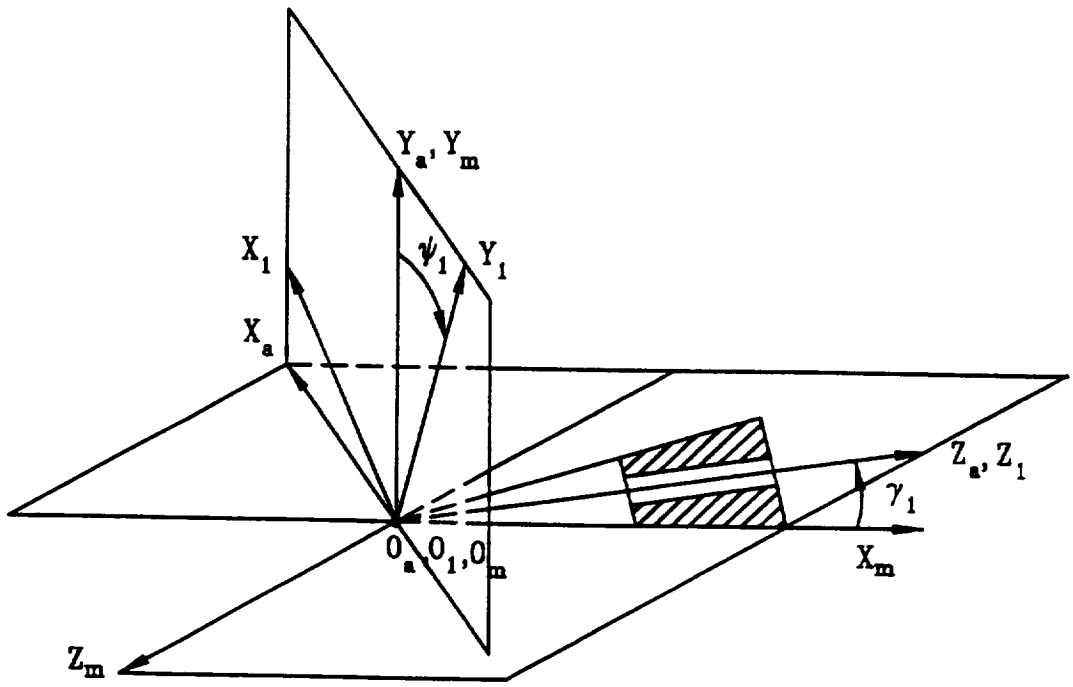

Fig. 8: Coordinate systems S_m, S_a and S_1

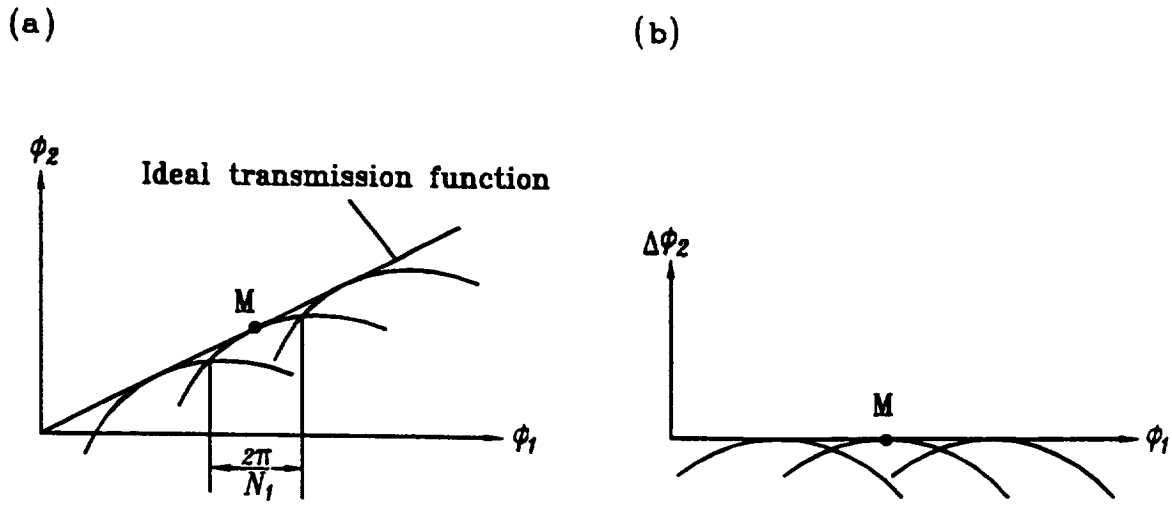

Fig. 9: Transmission function and predesigned parabolic function of transmission errors, ϕ_1-pinion rotation angle; ϕ_2-gear rotation angle; $\Delta\phi_2$-transmission error

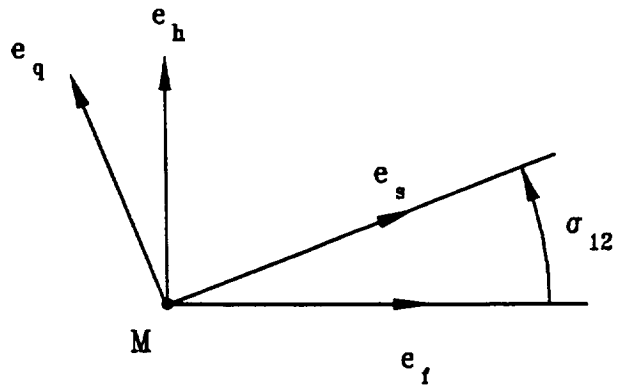

Fig. 10: Unit vectors of principal directions of surfaces Σ_2 and Σ_1

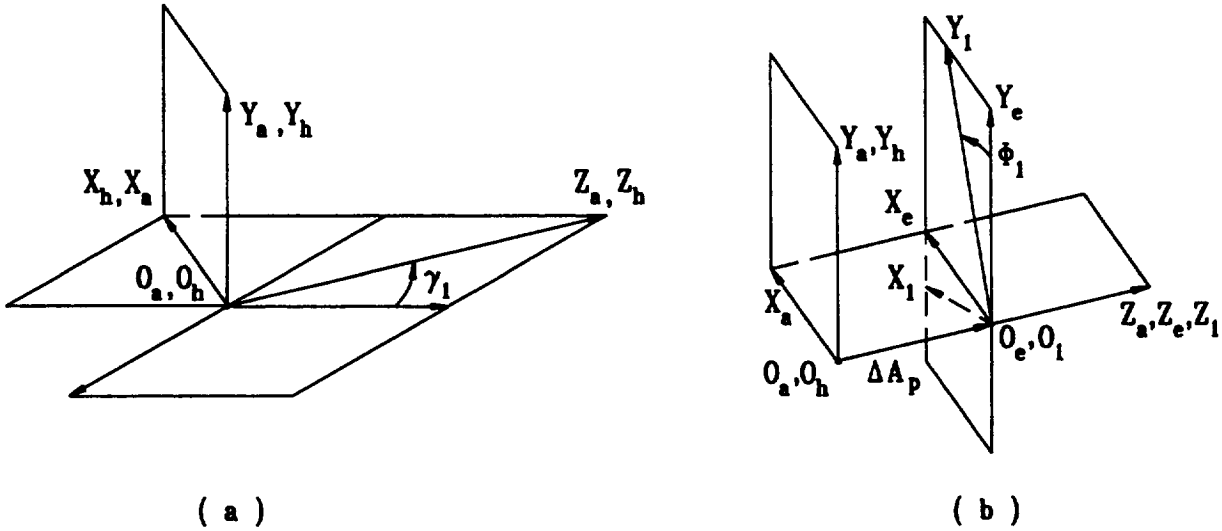

Fig. 11: Simulation of pinion misalignment ΔA_p

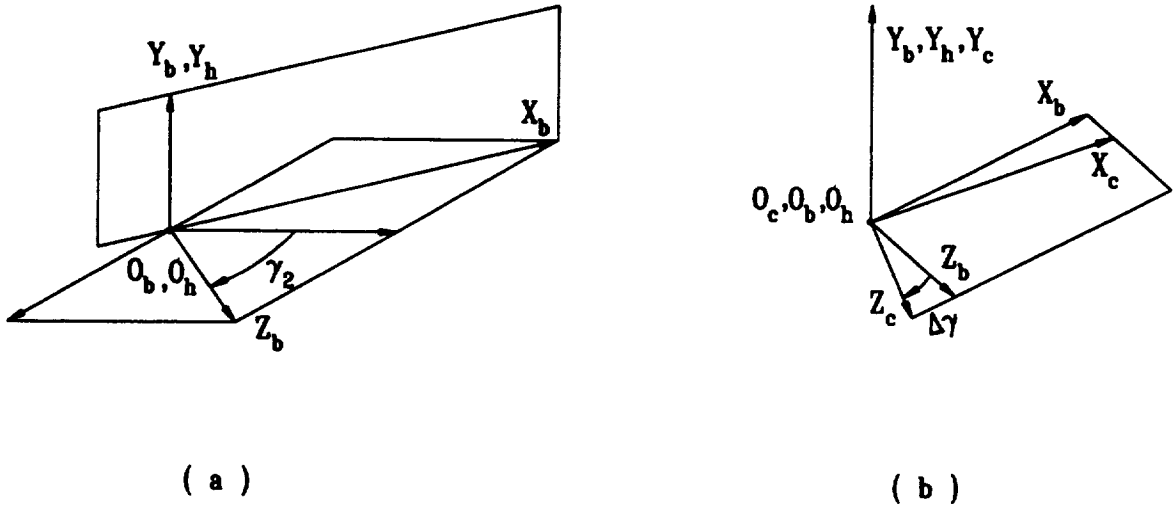

Fig. 12: Simulation of gear misalignment $\Delta\gamma$

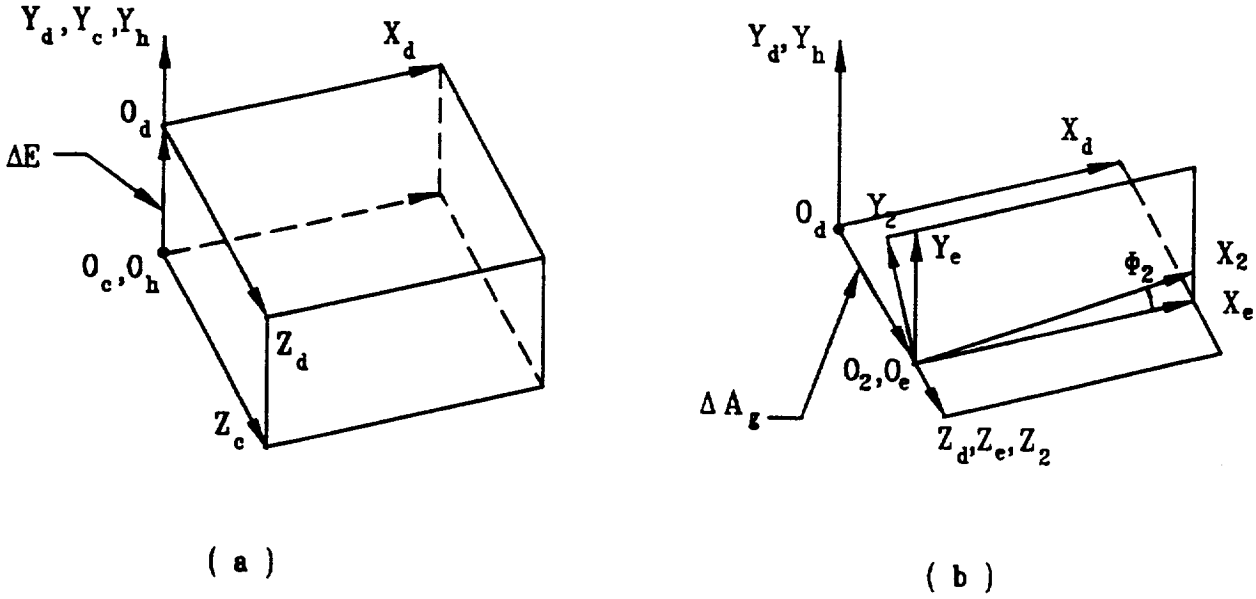

Fig. 13: Simulation of gear misalignment ΔE and ΔA_g

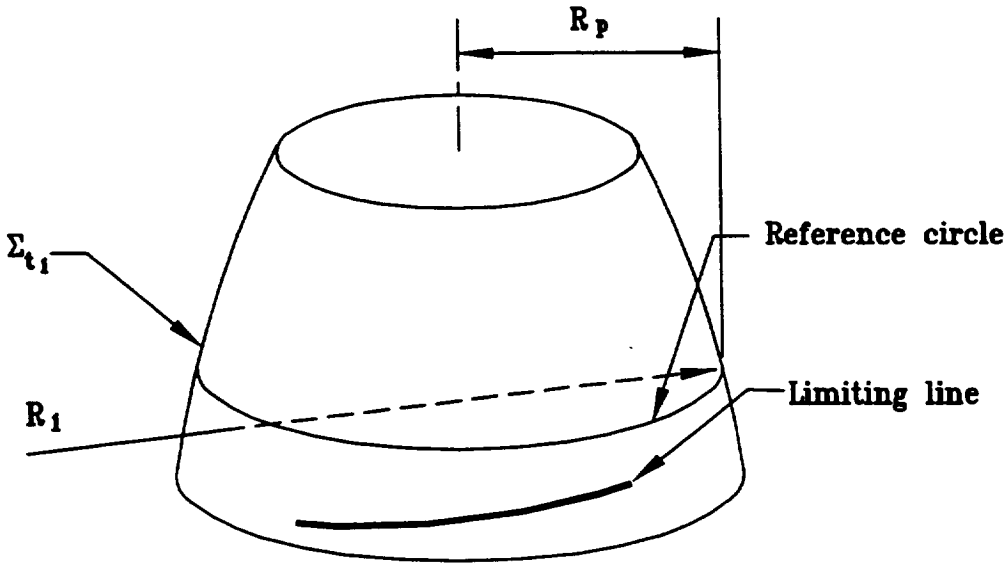

Fig. 14: Limiting line on generating surface of revolution

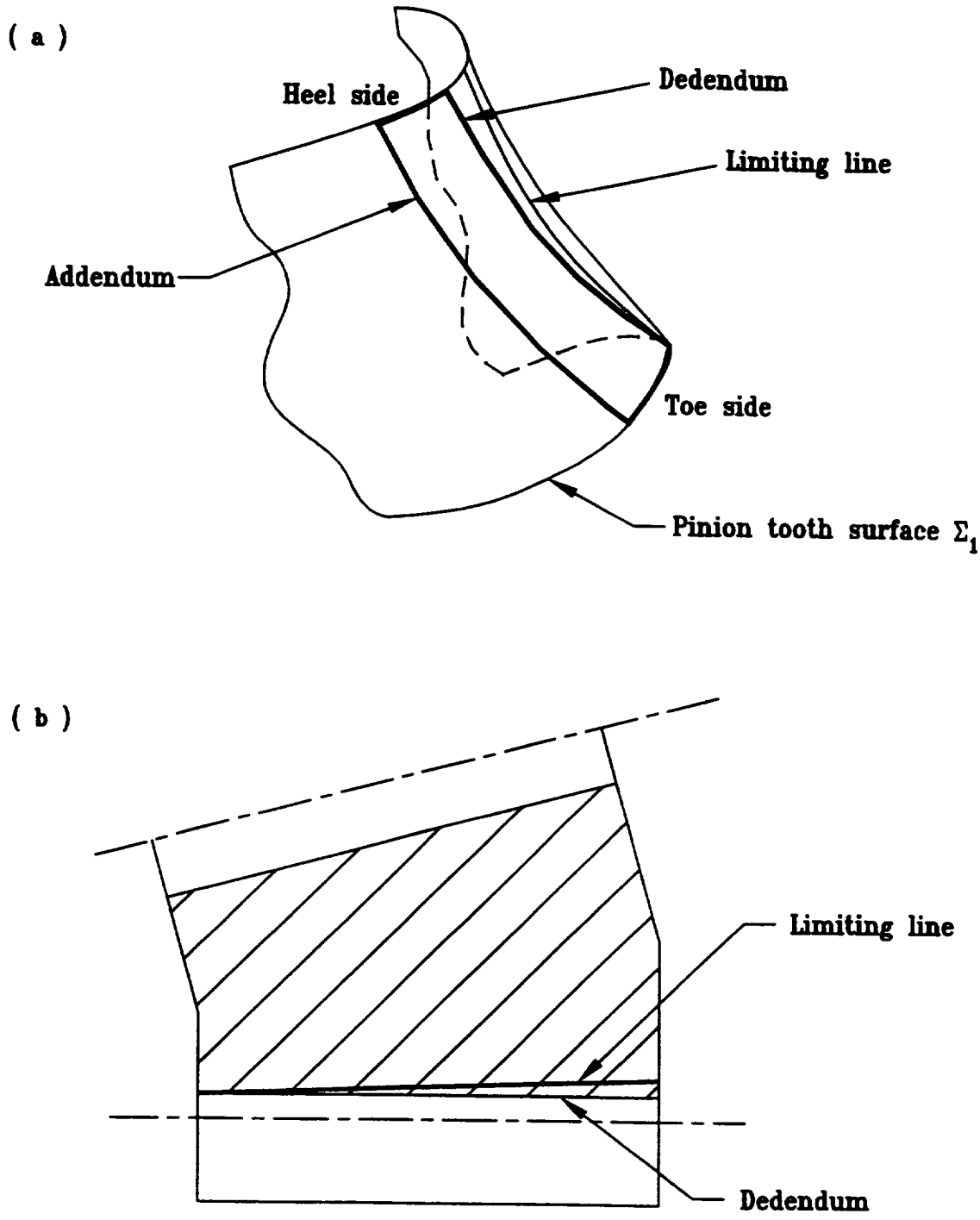

Fig. 15: Limiting line on pinion tooth surface

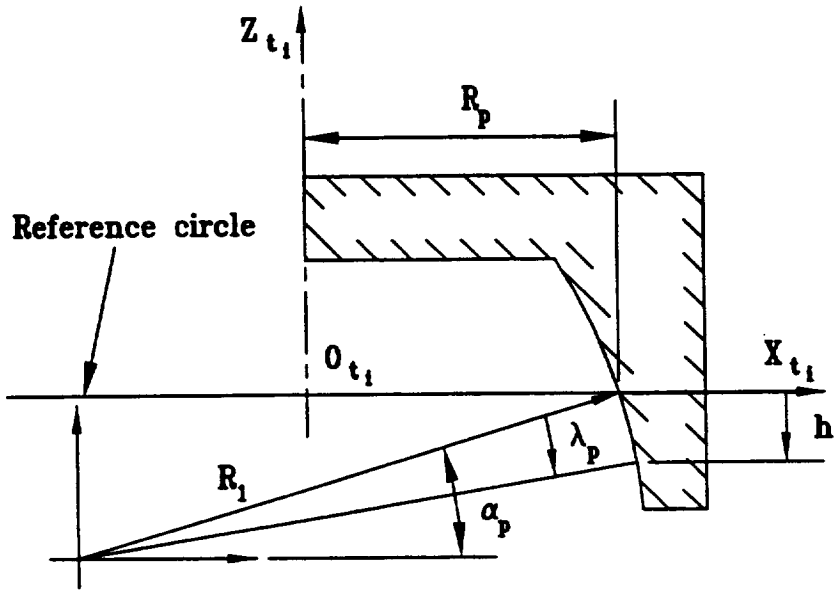

Fig. 16: For the derivation of the limiting value of the dedendum

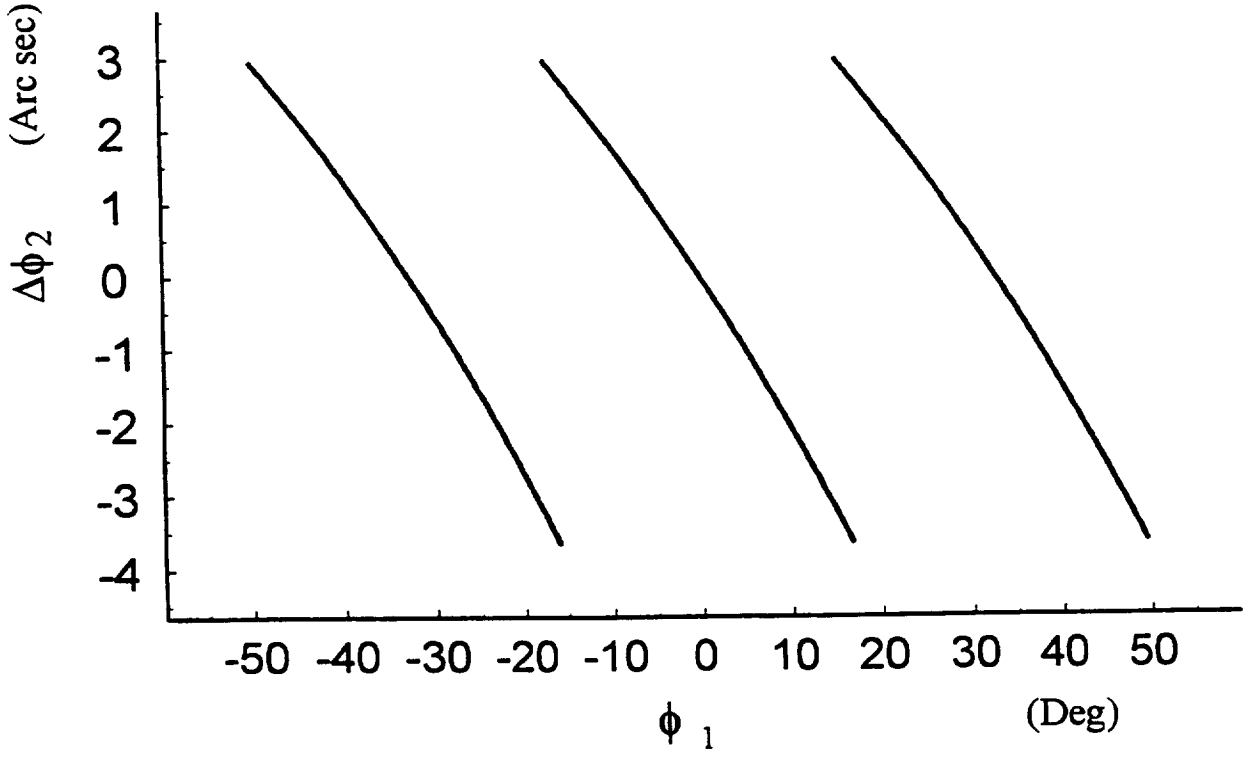

Fig. 17: Transmission errors for a misaligned gear drive with ideal surfaces: $\Delta\gamma = 3$ arc min.

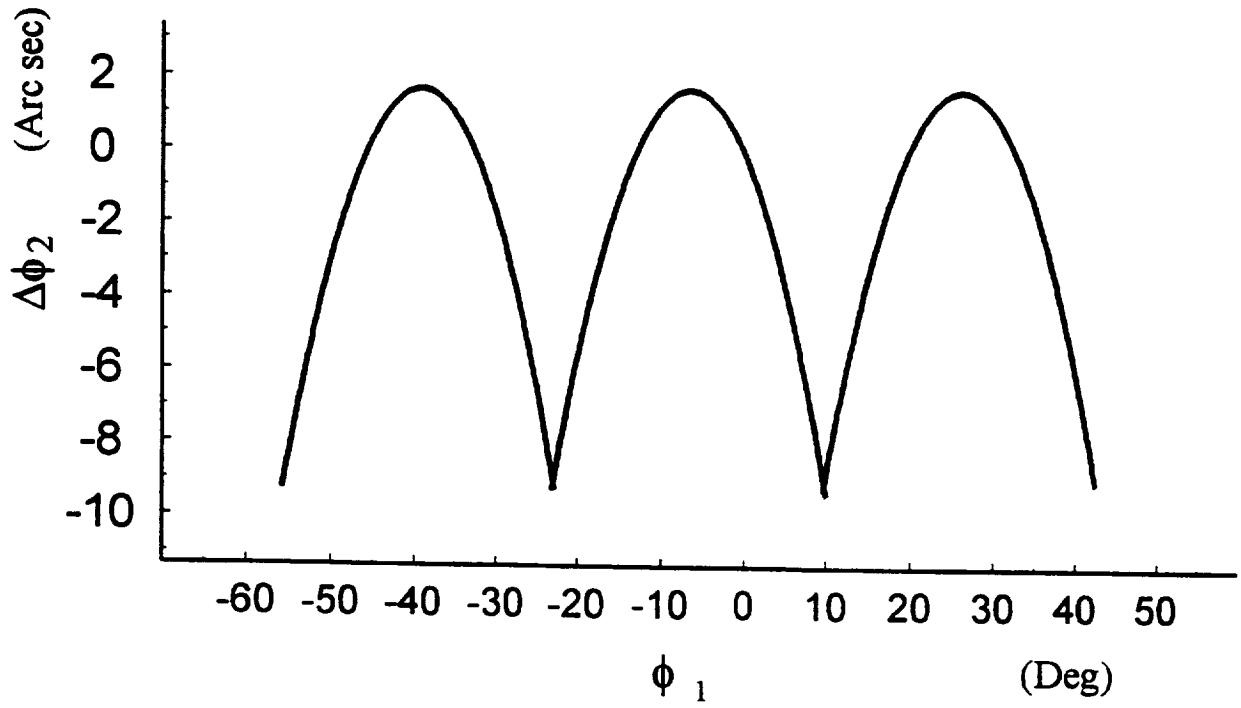

Fig. 18: Transmission errors for a misaligned gear drive with mismatched gear tooth surfaces: $\Delta\gamma = 3$ arc min.

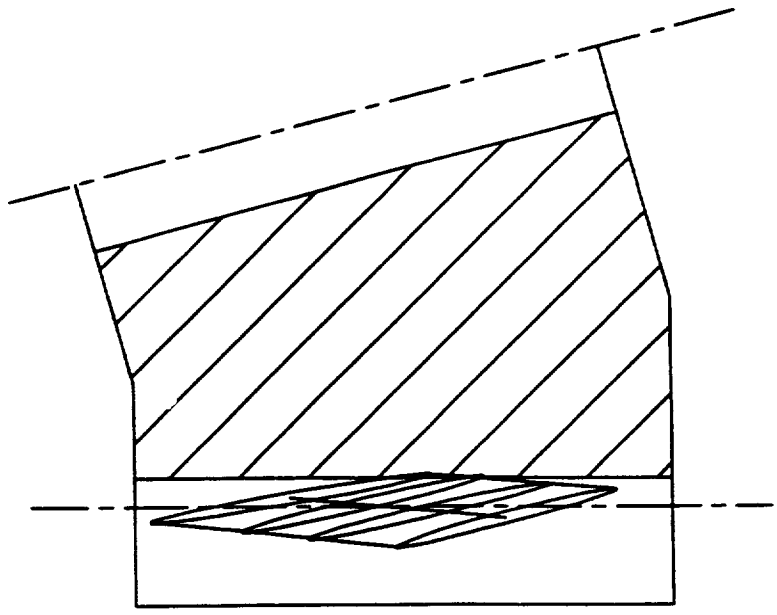

Fig. 19: Longitudinal bearing contact for a misaligned gear drive ($\Delta\gamma = 3$ arc min.)

REPORT DOCUMENTATION PAGE

Form Approved
OMB No. 0704-0188

1. AGENCY USE ONLY (*Leave blank*)	2. REPORT DATE	3. REPORT TYPE AND DATES COVERED
	October 1996	Final Contractor Report

4. TITLE AND SUBTITLE

Local Synthesis and Tooth Contact Analysis of Face-Milled, Uniform Tooth Height Spiral Bevel Gears

5. FUNDING NUMBERS

WU-505-62-36
1L162211A47A

6. AUTHOR(S)

F.L. Litvin and A.G. Wang

7. PERFORMING ORGANIZATION NAME(S) AND ADDRESS(ES)

University of Illinois at Chicago
Department of Mechanical Engineering
Chicago, Illinois 60680

8. PERFORMING ORGANIZATION REPORT NUMBER

E-10482

9. SPONSORING/MONITORING AGENCY NAME(S) AND ADDRESS(ES)

Vehicle Propulsion Directorate
U.S. Army Research Laboratory
Cleveland, Ohio 44135-3191
and
NASA Lewis Research Center
Cleveland, Ohio 44135-3191

10. SPONSORING/MONITORING AGENCY REPORT NUMBER

NASA CR-4757
ARL-CR-312

11. SUPPLEMENTARY NOTES

Project Manager, Robert F. Handschuh, Vehicle Propulsion Directorate, U.S. Army Research Laboratory, NASA Lewis Research Center, organization code 0300, (216) 433-3969.

12a. DISTRIBUTION/AVAILABILITY STATEMENT

Unclassified - Unlimited
Subject Category 37

This publication is available from the NASA Center for AeroSpace Information, (301) 621-0390.

12b. DISTRIBUTION CODE

13. ABSTRACT (*Maximum 200 words*)

Face-milled spiral bevel gears with uniform tooth height are considered. An approach is proposed for the design of low-noise and localized bearing contact of such gears. The approach is based on the mismatch of contacting surfaces and permits two types of bearing contact either directed longitudinally or across the surface to be obtained. Conditions to avoid undercutting were determined. A Tooth Contact Analysis (TCA) was developed. This analysis was used to determine the influence of misalignment on meshing and contact of the spiral bevel gears. A numerical example that illustrates the theory developed is provided.

14. SUBJECT TERMS	15. NUMBER OF PAGES
Transmissions; Gears; Gear geometry	49
	16. PRICE CODE: A03

17. SECURITY CLASSIFICATION OF REPORT	18. SECURITY CLASSIFICATION OF THIS PAGE	19. SECURITY CLASSIFICATION OF ABSTRACT	20. LIMITATION OF ABSTRACT
Unclassified	Unclassified		